Sensorless method of detecting plunger position in solenoid actuators

Simon Hed

Axel Knutsson

LUND UNIVERSITY

Department of Automatic Control

MSc Thesis
TFRT-6097
ISSN 0280-5316

Department of Automatic Control
Lund University
Box 118
SE-221 00 LUND
Sweden

Printed in Sweden by Tryckeriet i E-huset
Lund 2020

Abstract

This thesis investigates if it is possible to measure the plunger position in a Ledex 282352-023 solenoid actuator without the use of external sensors. To do this, various different methods, all based on comparing the current response to the applied voltage were evaluated from different categories such as calculation time, reliability and distinct position levels. The method that performed best in these categories was to calculate the phase difference between the voltage and the current using Fourier coefficients (FC). Model-based programming with MATLAB and Simulink was used to evaluate the performance of the methods. The Simulink model which implemented FC as measurement method is described in detail in this thesis. To run the models in real-time, hardware and software from dSpace were used which includes a MicroAutoBox II (MAB) and the program ControlDesk. This thesis was conducted in collaboration with BorgWarner.

Acknowledgements

Firstly we would like to thank BorgWarner for the opportunity to do our master thesis with them. Special thanks to our supervisors Johan Blomberg and Arne Hörberg alongside Hans Aulin for providing ideas and feedback for the measurement methods. We also want to thank Björn Helander and Jon Axelsson for providing useful equipment. Johan and Arne have really tried to give us the best opportunities to make this in to a good thesis. Secondly we want to thank our supervisor Prof. Anders Robertsson and examiner Prof. Rolf Johansson from the Department of Automatic Control at Lund University. Without Anders great feedback from the weekly meetings this thesis would not have been possible. We would also like to express our gratitude to Johan Björnstedt from IEA for the informative discussions about the solenoid and magnetic circuits. Finally we would like to thank Getachew Darge from IEA for giving us access to measurement related equipment.

Contents

Acronyms

AC Alternating Current

ADC Analog-to-Digital Converter

DC Direct Current

DFT Discrete Fourier Transform

emf Electro-Motive Force

FC Fourier Coefficients

FFT Fast Fourier Transform

LS Least-squares estimation

MAB MicroAutoBox II

MHEV Mild Hybrid Electrical Vehicle

PHEV Plug-in Hybrid Electrical Vehicle

PWM Pulse Width Modulation

RTI Real-Time Interface

1

Introduction

1.1 Background

A mild hybrid electrical vehicle (MHEV) is a vehicle that contains at least one electrical source of power, and at least one power source of a different type. Most commonly there is one of each where the electrical source is a motor and the other source is a combustion engine. The electrical motor is reversible which means that the battery that is supplying the electrical motor can be charged when the vehicle is breaking. In contrast to a Plug-in hybrid electric vehicle (PHEV) the MHEV does not have an outlet to allow the battery to be charged externally. Charging the battery when breaking conserves energy that would otherwise have been wasted, which improves fuel economy. The MHEV in the scope of this thesis uses motor configuration P3. This means that the electrical motor is connected to the output shaft of the transmission as seen in Figure 1.1 [Eckenfels et al., 2018; Fung, 2014]. The

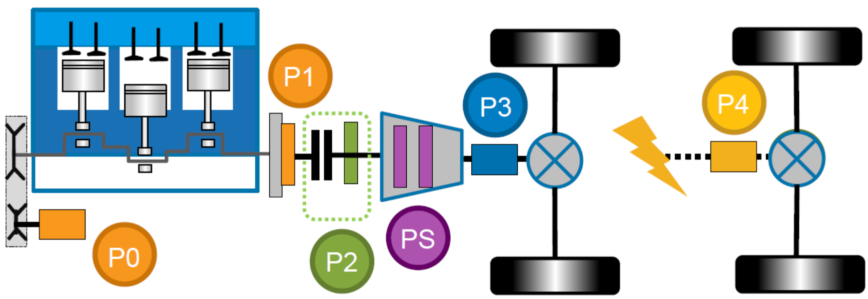

Figure 1.1 Architecture of hybrid cars. Picture from BorgWarner.

electrical motor used in the scope of this thesis is rated for a maximum of 20kRPM. This is an issue because when the vehicle is travelling at 140km/h the rotational speed of the output shaft of the transmission is approximately 20kRPM. To prevent that the electrical motor takes damage or is destroyed when the vehicle is travelling at 140km/h or higher a dog clutch can be used to disconnect the motor. For the vehicle in the scope of this thesis, the dog clutch is actuated using a solenoid actuator. There is always a small risk of the clutch not being correctly connected or disconnected, independently of which actuation method being used. BorgWarner is a company constantly looking for ways to improve safety and detectability, therefore it is desired to be able to detect that the clutch have been connected or disconnected properly. When a solenoid actuator is used this could be done by measuring the position of the solenoid plunger. It is desired to not use sensors for this position measurement, instead information from how the current respond to the applied voltage will be used to estimate the position. This is because sensors adds extra cost and requires special handling both in electronic and software design and sometimes increase complexity of the system.

1.2 Master thesis goals

The main goal of this master thesis is to find an optimized way to determine the position of the plunger in a solenoid actuator. The solenoid used in this thesis is a Ledex 282352-023. The position has to be estimated at least once every 100ms. The range that the solenoid will be working in is 0-6mm. The solenoids plunger position is defined as shown in Figure 1.2. The position estimation must be able to handle different voltages since it will be powered by the same battery that is powering the electrical motor where the voltage can vary from 36-65V.

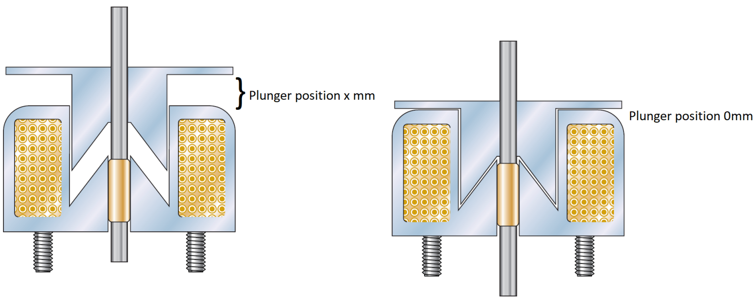

Figure 1.2 Plunger position definition.

Modified picture from datasheet: `https://www.johnsonelectric.com/-/media/files/solenoids-design-considerations/low-profile-design-considerations-metric.ashx?v=6501663582c64730a3fb34b332c3b026&la=en?v&hash=E65C59B4303B588CF4C2DBD20182E8425F1B756F"`

1.3 Individual contributions

Both students have contributed to the thesis and have worked alongside at Borg-Warner on a daily basis with information gathering and experiments.

1.4 Outline

Chapter 2 - Theory
Here the theory describing how it is possible to extract information about the solenoids plunger position by measuring how the current respond to the applied voltage is presented.

Chapter 3 - Modeling
Presents the experimental setup and Simulink models.

Chapter 4 - Result
The result for the performance of the measurement methods is shown.

Chapter 5 - Discussion
In this chapter the advantages and disadvantages of each measurement method are discussed.

Chapter 6 - Conclusion and future work
Here the best measurement method is presented based on the discussion in chapter 5. In the future work section in this chapter, possible improvements and additional features that should be implemented are presented.

2

Theory

2.1 Actuation of the solenoid

The solenoid is actuated using Pulse Width Modulation (PWM). PWM is used to limit the average energy that is provided to a system by opening and closing a switch that is connected between the system and the power supply. The ratio of on time compared to off time is called duty cycle. In most of the measurement methods investigated in this thesis, a sinusoidal scan signal is applied to the solenoid to allow position detection. This sinusoidal scan signal is generated by oscillating the PWM duty cycle in a sinusoidal pattern [Dee, 2013]. This is illustrated in Figure 2.1, Figure 2.2 and Figure 2.3. Notice that the duty cycle in these figures is oscillated between 0-50%, this will from here on be referred to as "scan signal duty 50%".

The solenoid is going to have three modes of actuation. To better understand these modes the reader is suggested to take a look at Figure 2.4 which shows how the solenoid is going to be connected to the return spring. First there is the non-actuated mode where the solenoid plunger is pushed to position 6mm by the return spring. In this mode the PWM duty cycle will only consist of a scan signal to allow position measurement. Secondly there is the holding-mode where the solenoid plunger is at position 0mm, here the actuation signal will consist of both the scan signal and a base duty cycle (constant offset added to the scan duty every cycle) to keep the return spring compressed. Finally there is the kick-mode where the return spring is to be compressed, here the actuation signal only consists of a large base duty cycle to quickly assert great force on the solenoid plunger. Measuring the position in the kick-mode is outside of the scope of this thesis.

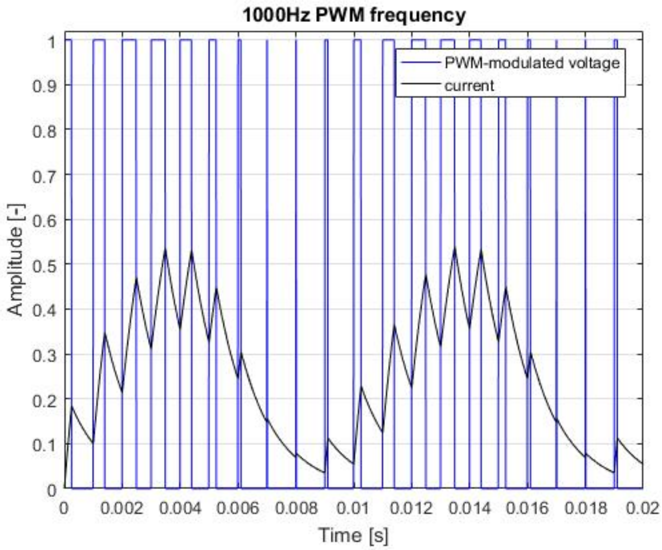

Figure 2.1 An illustration of the current resolution at 1000Hz PWM frequency.

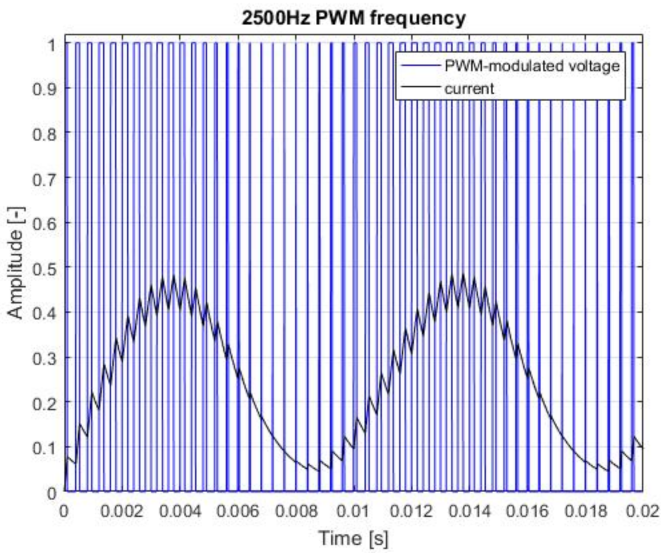

Figure 2.2 An illustration of the current resolution at 2500Hz PWM frequency.

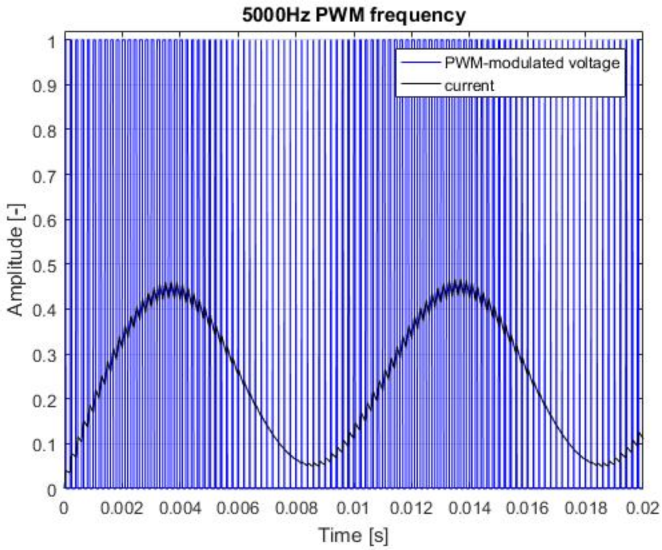

Figure 2.3 An illustration of the current resolution at 5000Hz PWM frequency.

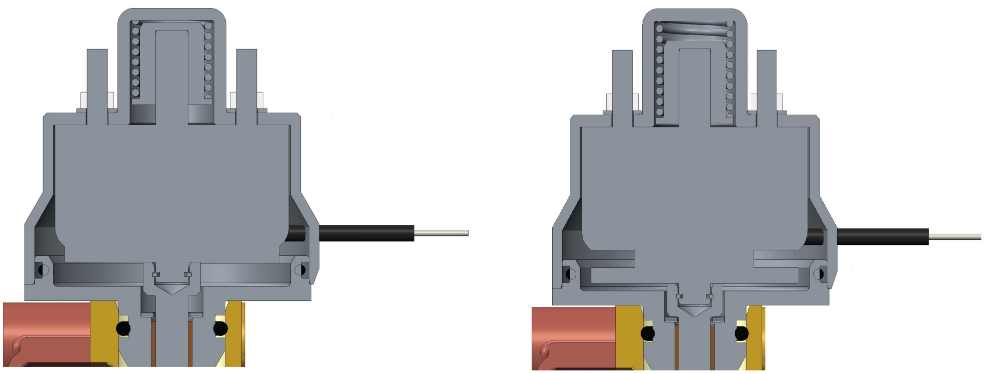

Figure 2.4 (**left**) Return spring compressed, plunger position 0mm (clutch connected). (**right**) The solenoid plunger is pushed by the return spring to plunger position 6mm (clutch disconnected).

2.2 Inductance

If a wire is closely wound around a closed iron core the magnetic flux (Φ) inside the core is given by equation (2.1),

$$\Phi = \frac{N \cdot I}{\mathscr{R}} \tag{2.1}$$

where N is the number of turns the wire is wound around the core, I is the current running through the wire and $\mathscr{R}$ is the magnetic reluctance. The magnetic reluctance is dependent on the geometry and material of the core as shown in equation (2.2).

$$\mathscr{R} = \frac{l}{\mu \cdot A} \tag{2.2}$$

Here l is the length of the core, A is the cross section area of the core and μ is the absolute permeability of the core. The absolute permeability depends on the relative permeability and the permeability of free space as shown in equation (2.3).

$$\mu = \mu_r \cdot \mu_0 \tag{2.3}$$

Here μ_0 is the permeability of free space which is a constant ($1.26 \cdot 10^{-6}$H/m) and μ_r is the relative permeability which is dimensionless and dependent on the core material . For a ferromagnetic material μ_r is typically greater than 1000. If the core has an air gap that is short compared to the length of the core the magnetic reluctance can be approximated as in equation (2.4).

$$\mathscr{R} = (\frac{l_{fe}}{\mu \cdot A_{fe}} + \frac{l_{gap}}{\mu_0 \cdot A_{gap}}) \tag{2.4}$$

From equation (2.4) it follows that the Reluctance $\mathscr{R}$ increases if the length of the air gap (l_{gap}) increases. The definition of inductance is shown in equation (2.5).

$$L = \frac{N \cdot \Phi}{I} \tag{2.5}$$

Combining equation (2.1) and equation (2.5) it is possible to express the inductance as in equation (2.6) [Cheng, 2013].

$$L = \frac{N^2}{\mathscr{R}} \tag{2.6}$$

The solenoid consists of an iron core with an air gap. This can be seen in the cross section view in (2.5). The length of the air gap is dependent on the plunger position. This makes the magnetic reluctance depend on the plunger position, which in turn makes the inductance depend on the plunger position.

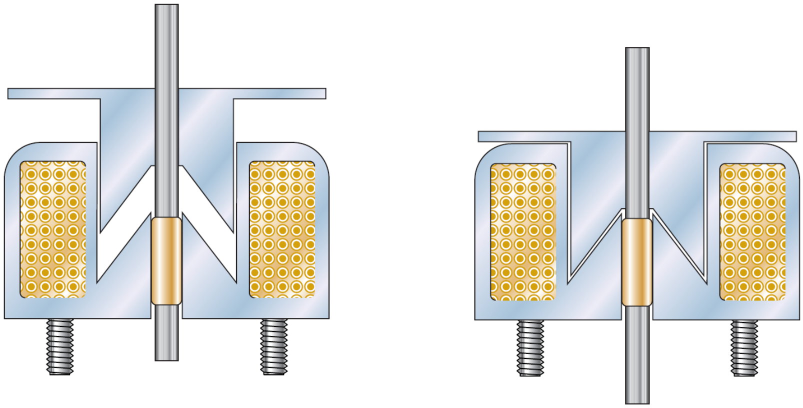

Figure 2.5 Cross section view of the solenoid.

Picture from datasheet: `https://www.johnsonelectric.com/-/media/files/solenoids-design-considerations/low-profile-design-considerations-metric.ashx?v=6501663582c64730a3fb34b332c3b026&la=en?v&hash=E65C59B4303B588CF4C2DBD20182E8425F1B756F"`

2.3 Temperature dependency

The resistance in the copper winding is temperature dependent and for temperatures between -50°C and 100°C it is assumed to be linear with an error less than 1%. The linear equation for the resistance is

$$R(T) = R_{ref}(1 + \alpha(T - T_0)) \tag{2.7}$$

where R_{ref} is the reference resistance 4.69Ω at temperature T_0 = 20°C and α is a material constant which is 0.00393K^{-1} for copper [Bruyne and Currat, 2015]. The solenoids characteristics are also dependent on the temperature of the core, however explaining the theory behind this dependency is outside the scope of this thesis.

2.4 The characteristics of the solenoid

Known parameters

Table 2.1 shows the known parameters of the solenoid.

Parameter	Notation	Value	Unit
Number of turns	N	567	-
Length of solenoid	l	31	mm
Weight	m	609.5	g
DC resistance for 20°C	R	4.69	Ω
Dielectric strength	E	1200	V/m
Area of wire	A	0.6	mm^2
Holding force at 105°C	F	218	N

Table 2.1 Known parameters of the solenoid.

Solenoid winding

Ideally the winding should be resistance free but this is not the case, but since copper has low resistivity the resistance is low enough to be suited for this kind of application [Spazini, 2001]. The resistance in the winding is also frequency dependent, this is called skin effect and increases with frequency. For low frequency there is almost only the dc resistance but for higher frequency the skin effect will affect the resistance more. The skin depth is described as

$$\delta = \frac{1}{\sqrt{f}} \tag{2.8}$$

where δ is the skin depth and f is the PWM frequency. Skin effect is effectively increasing the resistance by decreasing the area of the wire that the current is traveling in [Armstrong, 2018]. The equation for resistance is

$$R = \frac{l}{\sigma A} \tag{2.9}$$

where l is the length of the winding, σ is the conductivity and A is the area [Cheng, 2013]. So when the area decreases the resistance increases. This loss is not going to affect this thesis much since it is using PWM frequencies around 2500Hz.

Two additional small losses that will arise from the winding are the magnetic flux leakage and the proximity effect. Ideally the flux lines should all go through the material in the core but some will leak through the winding and isolation instead of going through the core and the amount of leakage is dependent on how many dislocations the material have [Lynch, 2009]. The next subsection will explain more about how dislocations are dealt with during the creation of the solenoid. Proximity effect describes how the parallel conductors in the winding affect each other. More specifically the proximity effect is described in [Potlabathini, 2015] as the effect that occurs when the AC current in two round, parallel wires is not distributed uniformly around the conductors. The magnetic fields from each wire affect the current flow in the other, resulting in a non-uniform current distribution, which in turn, increases the apparent resistance of the conductors.

Another property of the solenoid winding is the self induced electromotive force (emf) which is caused by change in the current flowing through the solenoid. When the current in the solenoid is changed the solenoid will oppose the current with a self induced emf. The current will create a magnetic field where energy is stored and when the solenoid is at maximum stored energy and the power supply is turned off, this energy will be used to maintain the current if there is an alternative path which a flyback diode adds. Eventually the current will drop to zero due to resistance in the circuit. This is described by Faradays's Law of Electromagnetic Induction and seen in equation (2.10) that can be derived to (2.11) [Cheng, 2013].

$$e = -N\frac{d\phi}{dt} \tag{2.10}$$

$$e = -L\frac{di}{dt} \tag{2.11}$$

Where e is emf in Volt, N is the number of turns, ϕ is the magnetic flux, L is the inductance and i is the current [Fitzpatrick, 2007b]. The equation for energy in an inductor can be seen in equation (2.12).

$$W = \frac{1}{2}Li^2 \tag{2.12}$$

Where W is the potential energy, L is the inductance and i is the current [Fitzpatrick, 2007a]. This means that disconnecting the power supply when a solenoid is fully charged creates a voltage spike in the same direction as the the current from the power supply is flowing in.

Solenoid core

A common way to model a solenoid with a circuit diagram is shown in Figure 2.6. The resistance R_m in Figure 2.6 is dependent on the solenoids core losses. The two most significant core losses are eddy currents and magnetic hysteresis.

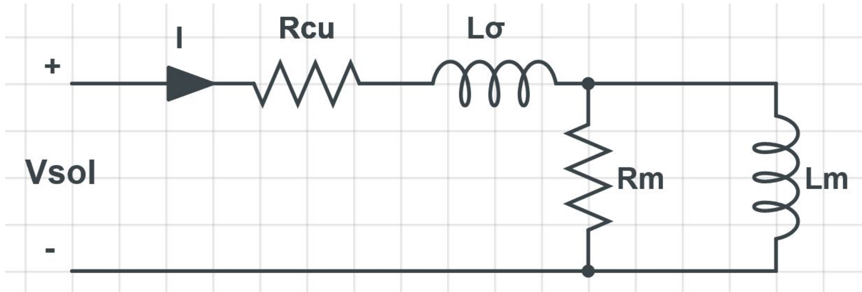

Figure 2.6 Solenoid circuit diagram where R_{cu} is the winding resistance, L_σ is the leakage inductance, L_m is the inductance from the flux lines passing through the core and R_m is the core losses modeled as a resistance.

Eddy current The power dissipation due to eddy currents increases with frequency squared. This can be derived using Ohms law, the equation for electric power and equation (2.10). When the solenoid plunger is at position 0mm the magnetizable part of the plunger will be exposed to a stronger switching magnetic field compared to when the magnetizable part of the plunger is located at a distance from the coil casing, this will result in higher power dissipation due to eddy currents which in turn will result in a plunger position dependency for the resistance R_m in Figure 2.6. [Cheng, 2013; Konda et al., 2017]. Figure 2.7 illustrates the principle how eddy currents are induced.

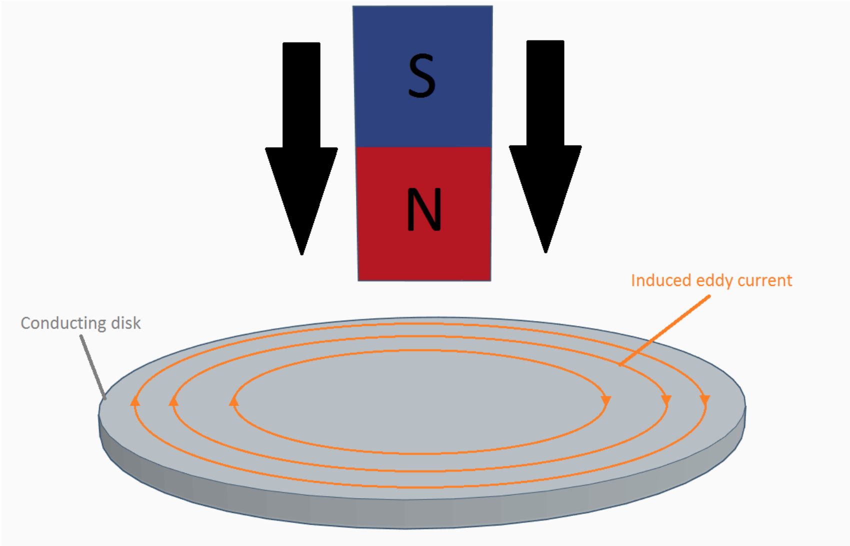

Figure 2.7 An Illustration of how eddy currents are induced in a conductive disc when the disc is exposed to a changing magnetic field.

Magnetic hysteresis The ferromagnetic core material has been through annealing which is a heating process where the material gets heated to the recrystallization temperature to make the material increase its ductility and reducing its hardness [Wojes, 2019]. Reducing the hardness makes the material decrease its magnetic coercivity and makes it less affected by hysteresis. Even though the core is now considered a soft material and contains few to none dislocations some domains does not lose alignment when the magnetizing field disappears. It is this phenomena that is called hysteresis and seen in Figure 2.8. If the system starts at the origin and the **H**-field is increasing then the magnetization will increase rapidly at first but then slow down until it reaches saturation. When decreasing the **H**-field the magnetization will follow the left curve and maintaining higher magnetization for lower **H**-field then at the system start. Eventually decreasing the **H**-field will saturate the magnetization again and to get the same level as the start a higher **H**-field is required than at the start [Urbaniak, 2012]. Since the amount of alignment depends on the past position and current this can also effect future states and positions. So measuring the position at 4mm can give different results having 3mm or 5mm as previous position [Cheng, 2013].

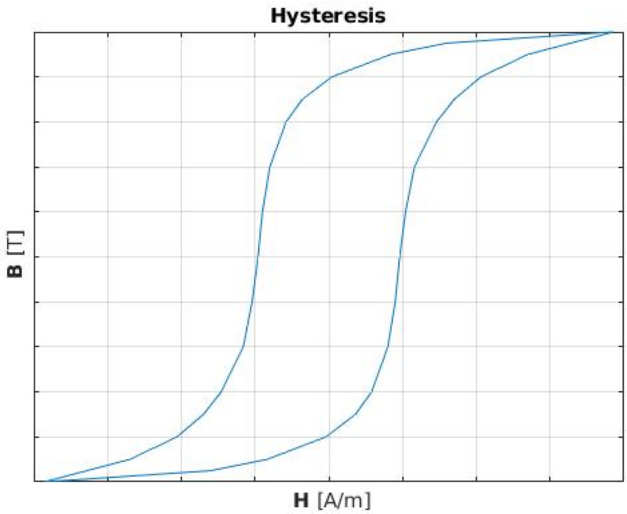

Figure 2.8 The figure shows the solenoids behaviour in a **B**-**H** plot.

Saturation Another impact of the solenoid having a magnetizable core is saturation. The saturation occurs when an increasing **H**-field can not further align the magnetic domains in the direction of the **H**-field. In the saturated region the solenoid will behave as if it had an air core, which corresponds to greatly reduced inductance compared to an unsaturated ferromagnetic core. In Figure 2.8 this can be seen since the curves derivative is going to zero when the **H**-field is increasing. The magnetic flux passing through the solenoid core is dependent on the length of the air gap. This results in that the solenoid will saturate at different current levels depending on the plunger position [Cheng, 2013].

2.5 The first-order RL circuit

The solenoid circuit diagram in Figure 2.6 can be rewritten to a simplified equivalent diagram as seen in Figure 2.9. When comparing the current response to the applied voltage it is possible to calculate L_s and R_s in Figure 2.9. It is then possible to experimentally map the values of L_s and R_s to the plunger position. In fact it is not even necessary to calculate L_s and R_s which require the use of both phase and magnitude. To acquire something that the plunger position can be mapped to it is sufficient to simply use either the phase or the magnitude value. The circuit in Figure 2.9 is called a first-order RL circuit. Using this model, the resulting impedance is given by equation (2.13). This impedance equation is fundamental for the majority of measurement methods investigated in this thesis.

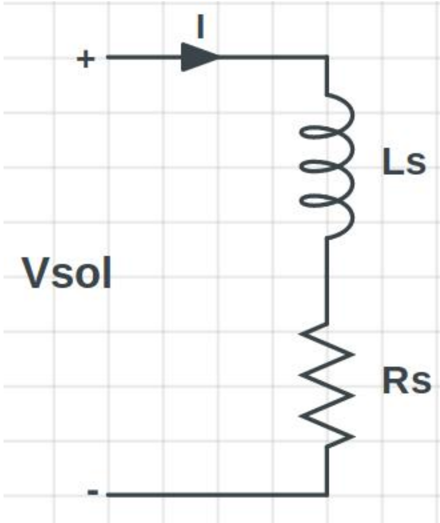

Figure 2.9 The solenoid modelled as a first order RL circuit.

$$Z = R + j\omega L \tag{2.13}$$

The step response of the RL circuit can be derived from equation (2.14) to equation (2.15) [Whiteley, 2002] where $t > 0$ and $I(0) = I_0$. Since the solenoid is to be actuated using PWM, important characteristics of the system can be described using the step response.

$$V = Ri + L\frac{di}{dt} \tag{2.14}$$

$$I_t = I_0 \cdot e^{(-Rt/L)} + (\frac{V}{R} \cdot (1 - e^{(-Rt/L)}) \tag{2.15}$$

In Figure 2.1, Figure 2.2 and Figure 2.3 the sinusoidal PWM oscillation and the current response when it is applied to an RL circuit is illustrated. This illustration was created using equation (2.15) with the parameters R = 47.2Ω and L = 0.0545mH. These parameters corresponds to the actual measured values of the solenoid at plunger position 0mm using a LCR meter with a scan frequency of 100Hz. Note that the current and voltage are normalized to improve visibility of the charging and discharging characteristics.

2.6 Measurement methods

In this section the theory behind the measurement methods that were investigated is presented. One of the methods, Fast Fourier Transform (FFT) is displayed under Phase-based methods throughout this thesis even though it could be used to extract information about the magnitude. This is because the information about the magnitude from FFT was never used.

Phase-based methods

As explained earlier in this chapter, the solenoids inductance and resistance is dependent on the plunger position. Depending on the ratio of the inductance and the resistance there will be a corresponding phase shift between the voltage and the current. This phase shift relates to the impedance as shown in equation (2.16). The theory behind the different methods that are based on this phase shift are presented in this subsection.

$$\text{phase shift} = \arctan\left(\frac{Z_{im}}{Z_{re}}\right) \tag{2.16}$$

The phase-based methods will use a sinusoidal signal with the frequency that was found out to be the best for FC with regards to phase. The method for selecting this scan signal frequency will be discussed in section: Frequency sweep.

Zero crossing One way to measure the phase difference between two sinusoidal waves is to identify where they intersect zero, and then calculate the difference between the times at the intersections. When the period time of the sinusoidal waves are known the phase difference is easily calculated by looking at the ratio between period time and difference in intersection time as in (2.17).

$$\text{phase shift} = \frac{\text{time shift}}{\text{period time}} \cdot 360 \tag{2.17}$$

Linear interpolation between the two measurement points with values closest to zero are used to estimate the time of intersection. The zero crossing method is illustrated in Figure 2.10 and Figure 2.11.

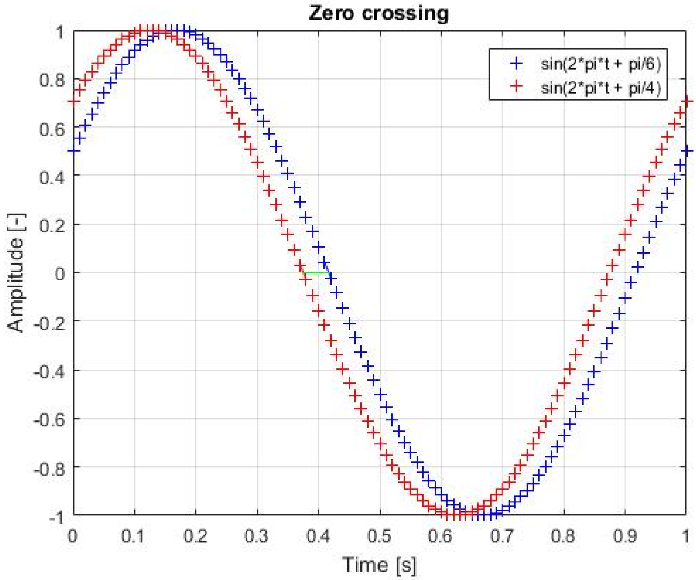

Figure 2.10 Zero crossing illustration.

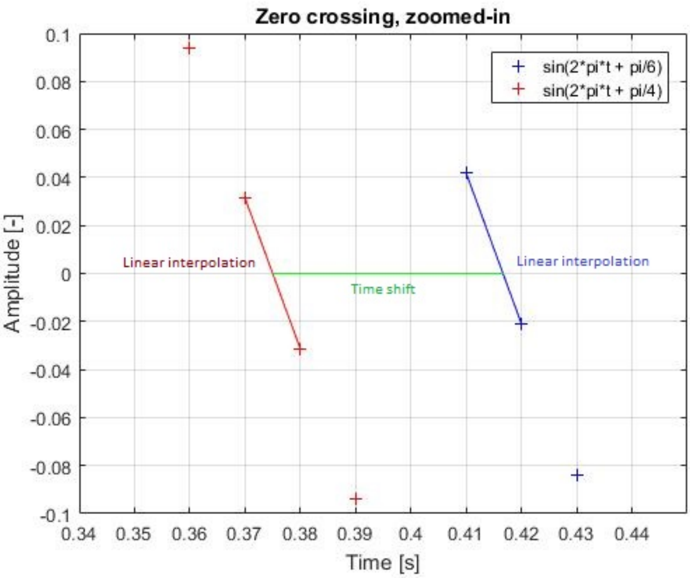

Figure 2.11 Zero crossing illustration, zoomed-in.

Fast Fourier transform FFT is an algorithm to calculate the discrete Fourier transform (DFT) [Weisstein, 2019b]. DFT is used to extract weights for the sine and cosine frequency components that a signal consists of. These weights (also known as FC) can later be used in a Fourier series to re-create the original signal. The FC could also be used to analyze the signal. In this thesis the signal that the FFT will be applied to is the sinusoidal scan signal. If the sampling time and number of sampling points are selected properly there will be a FC pair for the same frequency as the scan signal. This FC pair can then be used to extract phase and magnitude information of the scan signal. There are many different FFT algorithms, however, if the vector that FFT is applied to is a power of 2 there are specific algorithms that can reduce the amount of required computations. The algorithm MATLABs FFT function performs is dependent on the length of the vector it is applied to. One FFT algorithm that assumes that the vector length is a power of 2 is the Cooley–Tukey algorithm. The Cooley–Tukey algorithm reduces the number of computations needed for N points from $2N^2$ to $2N \cdot log_2(N)$ [Bekele, 2016]. The Cooley–Tukey algorithm first rearranges the input elements in bit-reversed order, then builds the output transform with the idea to break up a transform of length N into two transforms of length $N/2$. The Cooley–Tukey FFT algorithm is shown in equation (2.18) [Weisstein, 2019b].

$$\sum_{n=0}^{N-1} a_n e^{-2\pi jnk/N} = \sum_{n=0}^{N/2-1} a_n^{even} e^{-2\pi jnk/N} + e^{-2\pi jnk/N} \sum_{n=0}^{N/2-1} a_n^{odd} e^{-2\pi jnk/(N/2)}. \tag{2.18}$$

To get a FC pair with the same frequency as the scan signal the vector length and the sampling time that are used needs to be selected properly. They need to be selected so that exactly an integer multiple of the scan signal period fits inside the vector. An example of how FFT decomposes a signal is shown in Figure 2.12, Figure 2.13 and Figure 2.14. Figure 2.12 shows a signal that consists of three sinusoidal waves where the first have a frequency of 100Hz, an amplitude of 1 and a phase shift of 30°, the second have a frequency of 200Hz, an amplitude of 0.4 and a phase shift of 0°, and the third have a frequency of 300Hz, an amplitude of 0.7 and a phase shift of 130°. In Figure 2.13 the absolute value of the FC pairs are plotted and it is clearly seen that the signal in Figure 2.12 consists of three different components with frequency 100Hz, 200Hz and 300Hz. In Figure 2.14 the complex values of this wave are shown.

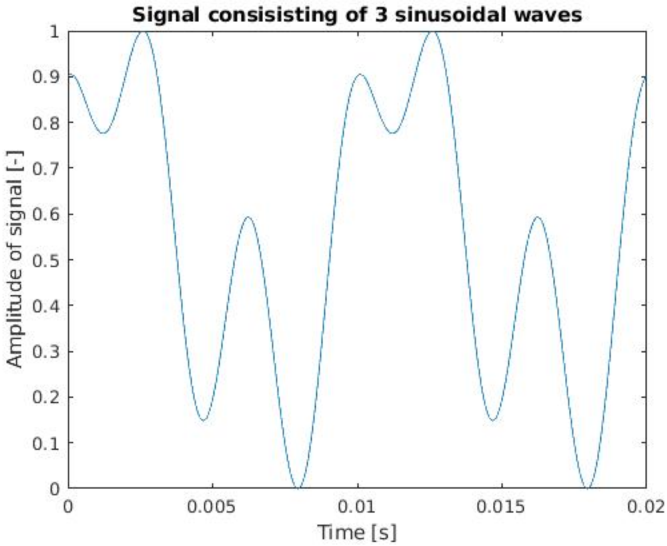

Figure 2.12 A normalized signal consisting of three sinusoidal waves where the first have a frequency of 100Hz, an amplitude of 1 and a phase shift of 30°, the second have a frequency of 200Hz, an amplitude of 0.4 and a phase shift of 0°, and the third have a frequency of 300Hz, an amplitude of 0.7 and a phase shift of 130°.

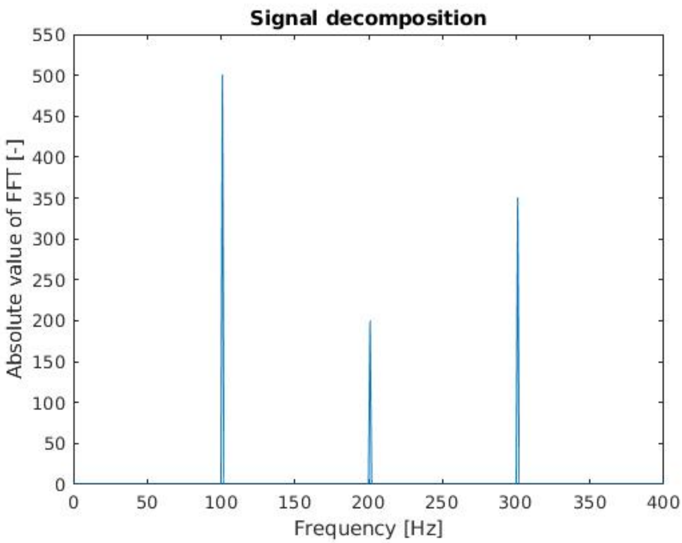

Figure 2.13 A decomposition of the unnormalized signal in Figure 2.12 using FFT.

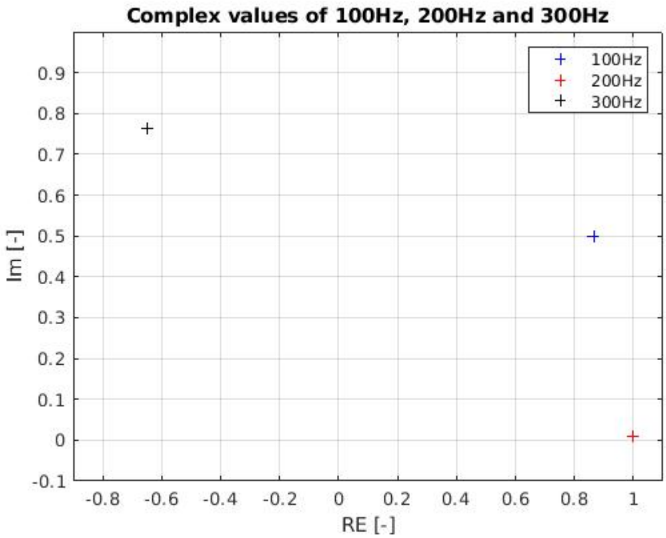

Figure 2.14 Normalized complex values of Figure 2.12 using FFT.

Convolution For a causal periodic signal $f(k)$ of length L and $g(k)$ with length N the convolution is given by

$$f \circledast g = \sum_{m=0}^{M-1} (f(k-m)g(m)) \tag{2.19}$$

where $M = N + L - 1$ and causal means that the signal is zero for negative time. This has the computational complexity of $\mathcal{O}(n^2)$. Using the Fast convolution algorithms (FCA) which uses FFT lowers the complexity to $\mathcal{O}(n \cdot log(n))$. The algorithm is performed by zero-padding the input and calculate the FFT, multiply them together and then take the inverse FFT [Spors, 2015]. The principle of convolution is shown is Figure 2.15 and Figure 2.16. The resulting vector can then be used to determine the phase by for example looking at what index corresponds to the highest value since index can be directly translated into time.

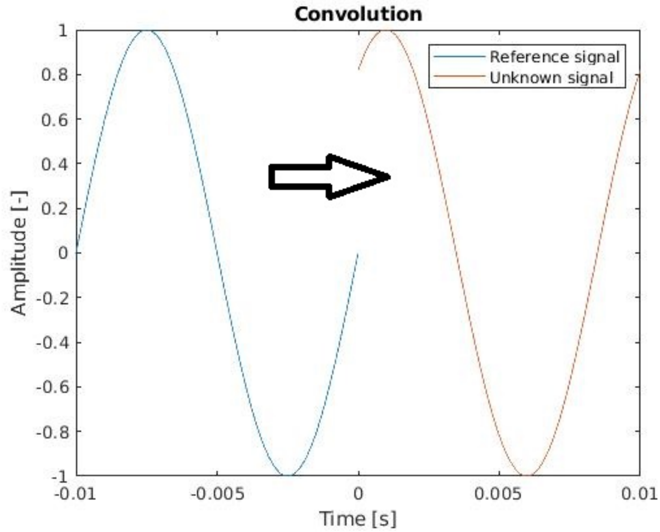

Figure 2.15 Illustration the start of performing convolution.

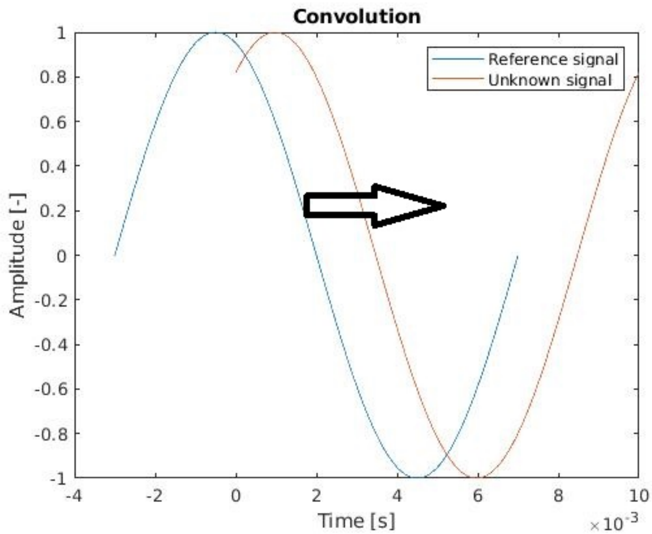

Figure 2.16 Illustration the middle of performing convolution.

Covariance Covariance measure the relationship between two random variables. For two variables the covariance is

$$COV[X,Y] = \frac{\sum_{i=1}^{n}(x_i - \bar{X})(y_i - \bar{Y})}{n} \tag{2.20}$$

where n is the number of data points, $\bar{X}$ is the mean of X and $\bar{Y}$ is the mean of Y [Weisstein, 2019a]. Knowing the phase difference between the voltage and the current at different plunger positions means that some predefined sinusoidal waves with phase corresponding to the different positions can be made. The covariance between the measured signal and one of the predefined sinusoidal waves will then be calculated in an iterative manner to find the best match. This implementation of covariance is similar to the method "Matched filter" which is a method that uses convolution between the measured signal and signal templates to detect the desired signal [Elm, 2019].

The different actuation modes are going to need to have their own set of predefined sinusoidal waves, since the phase shift is dependent on the actuation mode. In the non-actuated mode the outermost position and in the holding-mode the innermost position should be selected as starting points for an iteration, since these are the most likely positions to be at, which would limit the number required iterations to find the best match. This is illustrated in Figure 2.17 and Figure 2.18 where the unknown position would be determined to be 1mm with 1mm resolution.

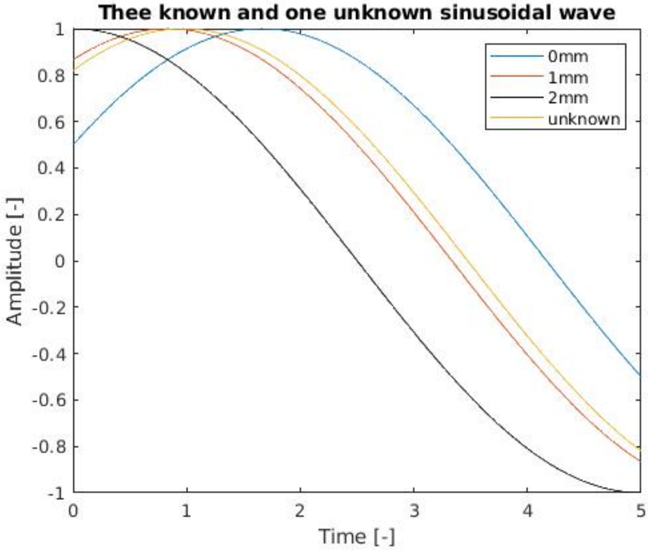

Figure 2.17 Four signals where there are three known that corresponds to expected phase for each position and one unknown that illustrates the sampled current.

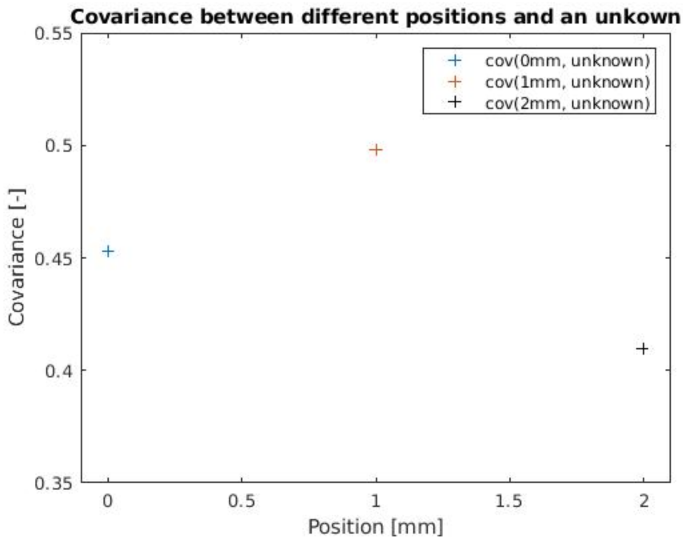

Figure 2.18 Covariance values of the different positions compared the the unknown current.

Magnitude-based methods

When the inductance and resistance increases, the current magnitude decreases. The magnitude of the current is dependent on the magnitude of the voltage divided by the magnitude of the impedance as seen in equation (2.21). The magnitude of the impedance can be calculated from the real and imaginary part of the impedance, this is seen in equation (2.22).

$$|I| = \frac{|V|}{|Z|} \tag{2.21}$$

$$|Z| = \sqrt{Z_{im}^2 + Z_{re}^2} \tag{2.22}$$

Current amplitude By measuring the minimum and the maximum value of a period of current, the amplitude can be calculated. If measurements from several periods are used a median-filter could be applied to remove abnormal measurements to provide a more reliable estimation. The principle of this method is shown in Figure 2.19 and Figure 2.20.

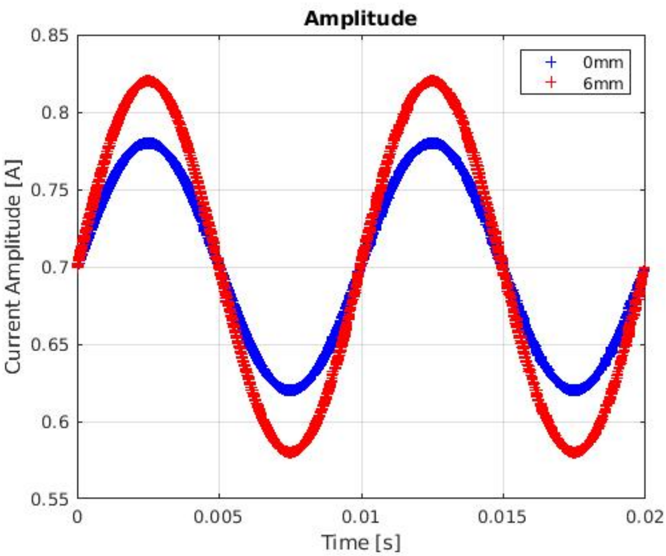

Figure 2.19 Amplitude illustration with an average current of 0.7A.

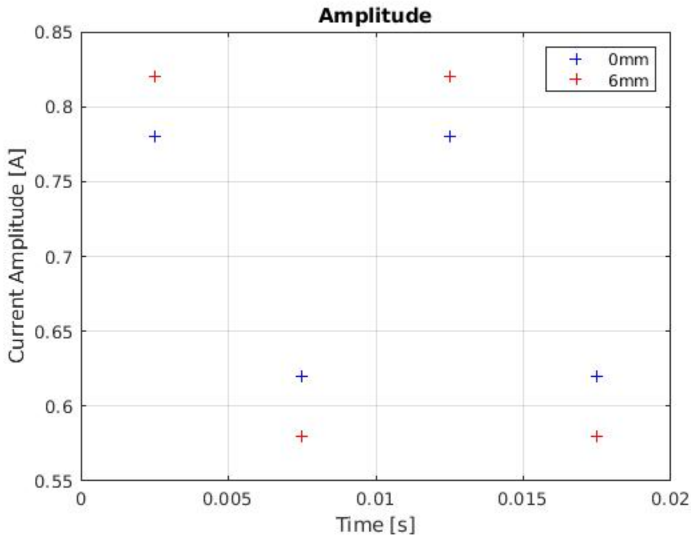

Figure 2.20 Amplitude illustration with only the min and max values.

Current integration The integration method is based on the same principle as the amplitude method. Compared to the amplitude method, the integration method is more robust since it is using all samples and is therefore not as affected from a single bad measurement. The integration process consists of three steps, first the dc-component of the current is removed using a filter, secondly the absolute value of the samples is computed, an example of what the current can look like at 0mm and 6mm after these two steps have been performed is seen in Figure 2.21. Thirdly the integration is performed. The area that is integrated can be seen in Figure 2.22 and Figure 2.23.

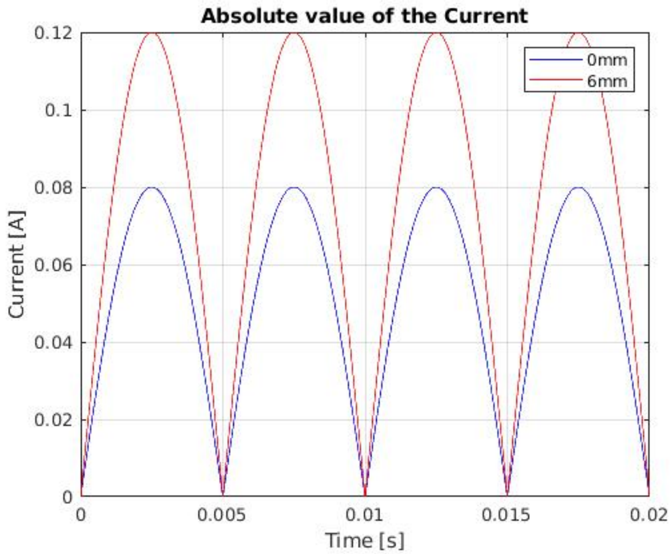

Figure 2.21 Absolute value of the samples for two different positions.

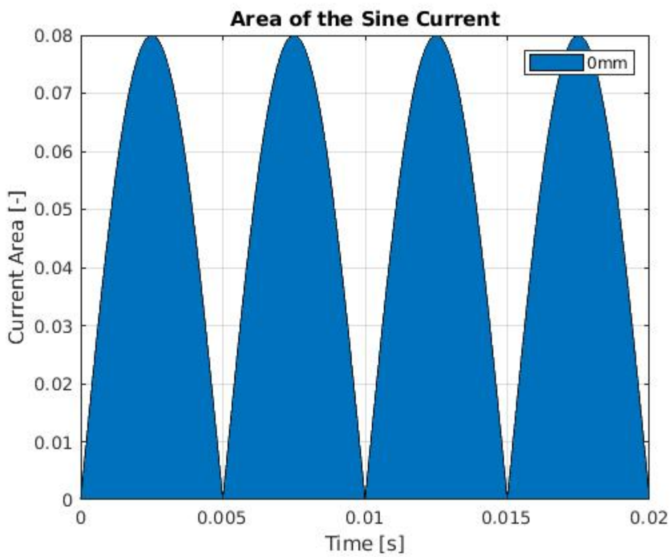

Figure 2.22 Illustration of the integrated area with a value of 1.019.

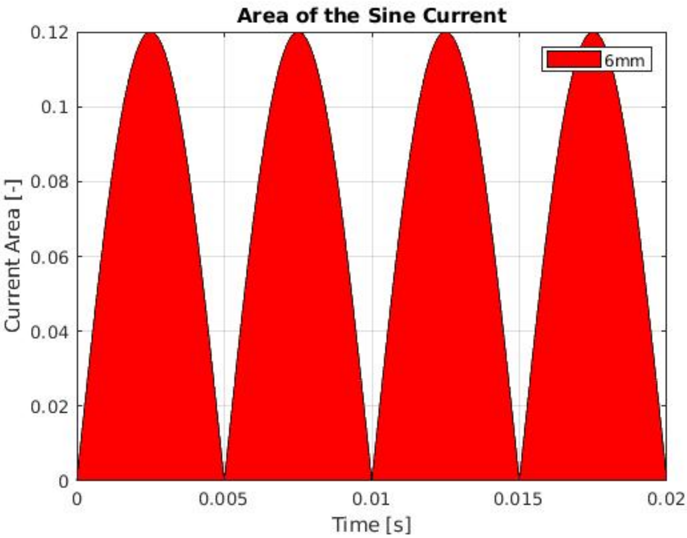

Figure 2.23 Illustration of the integrated area with a value of 1.527 .

Current control - Period Another measurement method that uses information about the magnitude of the impedance is the current control method. Here two set points are used to form a simple hysteresis controller. One is for the lower current limit and one is for the upper. The controller works in the following way: Initially the controller sends pulses to the solenoid with a fixed duty cycle until the current reaches the value of the upper set point. When this happens the duty cycle is set to zero and the current decays until it reaches the lower set point. Once this happens the duty cycle is changed back to the initial value and the current starts rising again. This pattern continues until the controller is turned off. When controlling the solenoid with this method information about the magnitude of the impedance is given by measuring the time it takes for the current to move between the set points.

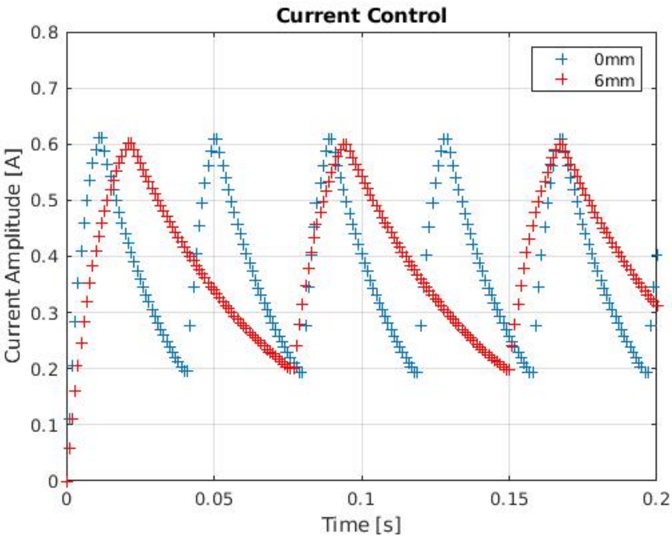

Figure 2.24 Current Control illustration from start with lower boundary at 0.2A and upper boundary at 0.6A.

Current control - Least-squares estimation Another variant of current control is to estimate the "time constant" using a LS approximation as seen in (2.24). The first step to derive this is to use equation (2.15) with $V = 0$ and $R/L = \tau$ and apply the natural logarithm to both sides. This is seen in equation (2.23).

$$ln(I_t) = -t\tau + ln(I_0) \tag{2.23}$$

Having

$$Y = \begin{bmatrix} ln(I_0) \\ ln(I_1) \\ \vdots \\ ln(I_n) \end{bmatrix} \quad , \quad A = \begin{bmatrix} -t_0 & 1 \\ -t_1 & 1 \\ \vdots & \vdots \\ -t_n & 1 \end{bmatrix}$$

and

$$X = \begin{bmatrix} \tau \\ ln(I_0) \end{bmatrix}.$$

Since Y and A are known X can be calculated using the matrix pseudoinverse

$$AX = Y => X = (A'A)^{-1}A'Y. \tag{2.24}$$

This variant is assumed to be better at handling noise since it uses more measurements points than the period variant and illustrated in Figure 2.25.

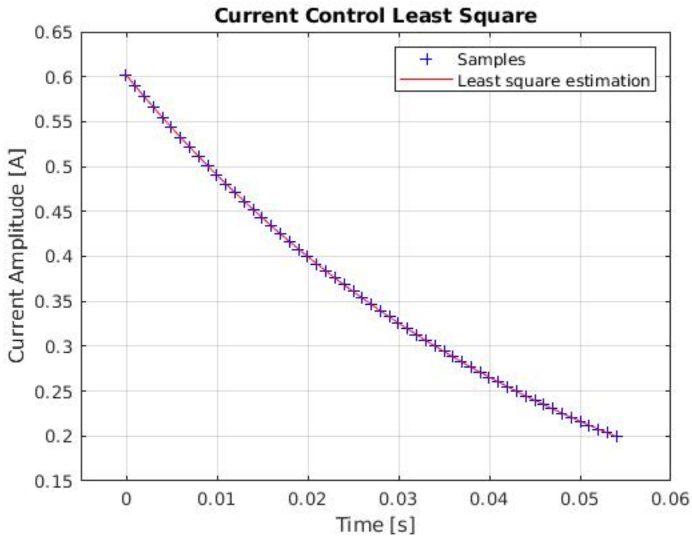

Figure 2.25 This figure shows the sample points and the LS estimation of the time constant in the slope.

Time constant

These methods does not use the sinusoidal scan signal like most of the others but looks more like current controls methods. Instead the time of high part of the PWM signal is held constant, and when the solenoid is supposed to be actuated, instead of increasing the on-part of the signal, the off-part time is reduced. When a solenoid is modelled as an inductance in series with a resistor the current passing through the solenoid is given by equation (2.15).

Time constant - Period In equation (2.15) the time constant is defined as shown in equation (2.25) [McAllister, 2016]. When a step in voltage is applied the solenoid current will begin to raise. After five time-constants the exponential term of equation (2.15) is so small that it can be neglected.

$$\tau = \frac{L}{R} \tag{2.25}$$

This method uses the principle of the time-constant by measuring the current twice every PWM period, once at the beginning of the high part and once at the end of the high part. The difference is then calculated. If the time for the on-part of the PWM is tuned correctly the difference can be used to calculate the inductance L. The tuning is done by setting the on time of the PWM to a maximum of five time constants, where the solenoid plunger is at position 0mm (where the inductance is highest). If this tuning is not performed no information is provided from the current difference at different plunger positions since the current will have time to raise to its steady-state value regardless of inductance related to a specific plunger position. The main advantage of this method is the fast rate of measurements. This method is illustrated in Figure 2.26 and Figure 2.27.

Time constant - Least-squares estimation This variation of the time constant method uses the fact that τ and $ln(I_0)$ can be estimated using LS similar using (2.24). So while it is similar to the other variation that it measured the current twice every PWM period, once at the beginning of the high part and once at the end of the high part, it also, at the same time, samples the current continuously (10MHz) which generated a vector of measurement similar to most of the methods. This vector is then used to estimate the time constant using the rise or the fall depending on which one gave the biggest difference in position. This can be seen by using the strategy in Figure 2.25 but for the rising slope of Figure 2.26 or Figure 2.27.

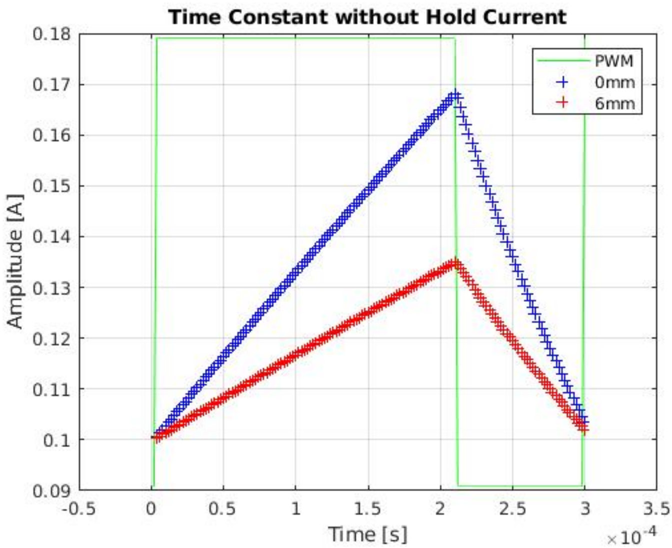

Figure 2.26 This figure shows the sample points of one PWM period using Time Constant method. This figure illustrates the non-actuated mode. The PWM low and high are just there for clarification and has nothing to do with the y-axis scale or unit.

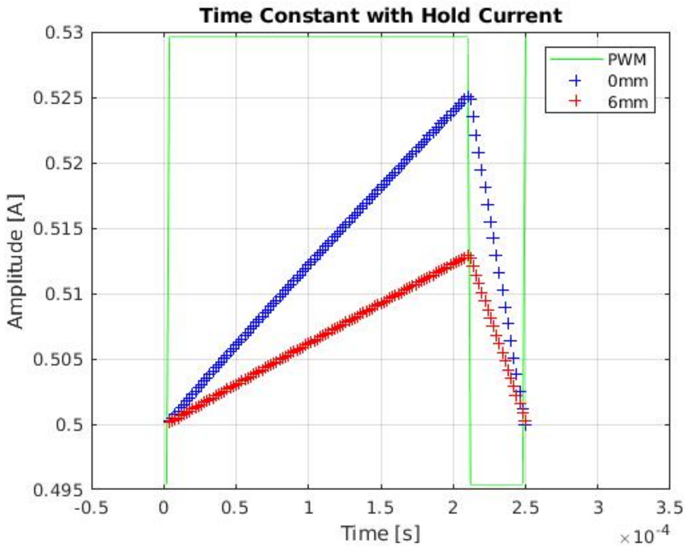

Figure 2.27 This figure shows the sample points of one PWM period using Time Constant method. This figure illustrates the holding-mode. The PWM low and high are just there for clarification and has nothing to do with the y-axis scale or unit.

Fourier coefficients

The FC pair for a single frequency is a subset of the DFT. Since the scan signal which the FFT or DFT should be applied to is a sinusoidal with a known frequency it is possible to calculate a single pair of FC to get the phase and magnitude information of the sinusoidal. For this method the magnitude is also investigated, this is why it is not listed under the Phase-based methods.

2.7 Frequency sweep

To find the best frequency for the sinusoidal scan signal a frequency sweep which investigated frequencies between 10Hz and 150Hz was conducted. Since the maximum measurement time is 100ms, the investigated frequencies were selected so that an integer multiple of periods could fit in the measurement time to get a FC pair for exactly the sought after scan signal frequency. For frequencies other than those which have an integer multiple of periods in the 100ms time span, the measurement time must be changed to still achieve an integer multiple of periods in the time span. The reason why 10Hz is the lowest frequency is that the maximum measurement time is 100ms which makes 10Hz the lowest frequency to still measure a complete period. The methods that will be used for this sweep will be FC for the phase and magnitude and also integration. The measurement itself will be 15s and then the difference between the 0mm position and 6mm position together with the variance will be the evaluation.

3

Experiments

3.1 Experimental arrangement

There were two different setups to perform different experiments using one solenoid each. One of the setups was used to be able to lock the solenoid plunger at a specific position to be able to conduct a position signal measurement at that position. This setup can be seen in Figure 3.2. In the other setup the solenoid was placed in the placeholder with spring, in this setup it was possible to investigate how much current was needed to keep the spring compressed. The solenoid placed inside the placeholder with spring can be seen in Figure 3.1. All the items that were used to perform the experiments are listed in Table 3.1. To perform the measurements, the measurement methods that is presented in the theory section had to be implemented in software. All the implementations were done in MATLAB/Simulink. With MATLAB coder, Simulink coder, and a C compiler, it was possible to generate code from a Simulink model which could run on the MAB. The MAB is a real-time system for performing fast function prototyping. All the softwares that were used in this thesis are listed in Table 3.2.

Items used for the experiments
21x 1mm screw washers
1x Gate driver
1x LCR meter
1x MicroAutoBox II
1x Oscilloscope
1x Placeholder with spring for solenoid
2x Power supplies
1x Stand for solenoid
2x Solenoids

Table 3.1 List of items used for the experiments.

Software used for the experiments
MATLAB
Simulink
ControlDesk
dSpace software for Simulink

Table 3.2 List of software used for the experiments.

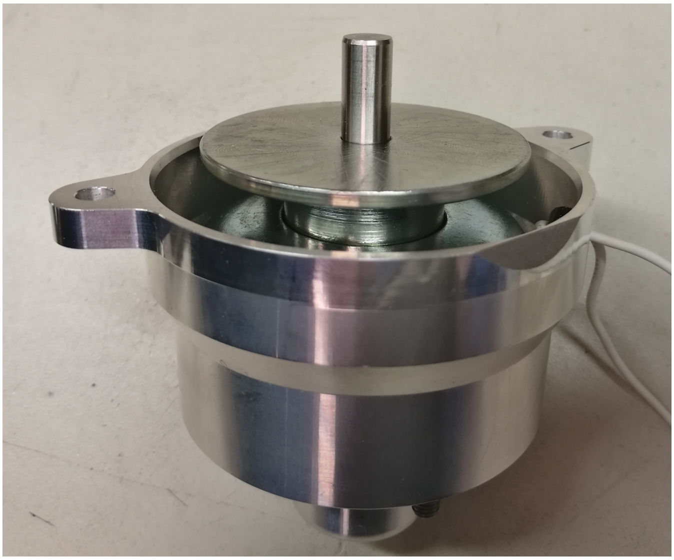

Figure 3.1 Here the solenoid is placed inside the placeholder with a spring.

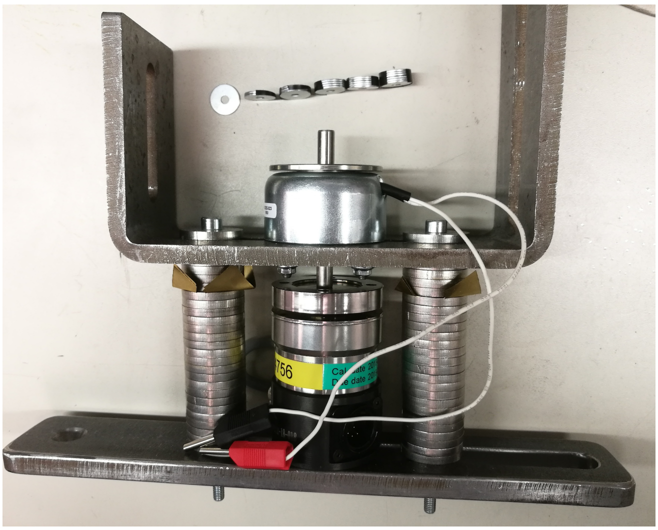

Figure 3.2 Here the solenoid, the washer groups and the stand are shown.

LCR meter

To better understand the behaviour of the solenoid, measurements was conducted using a LCR meter. The LCR meter was configured to assume that it conduced measurements on an RL circuit. This LCR meter used a voltage amplitude of 1.5V and had a tunable sinusoidal scan frequency. The LCR meter used is seen in Figure 3.3 and the model is Hioki IM3536 LCR Meter.

Figure 3.3 Here the LCR meter is shown. `https://www.hioki.com/en/information/detail/?id=159`

Gate Driver

The gate driver and the MAB together with the connection between them can be seen in Figure 3.4. The gate driver circuit diagram can be seen in Figure A.1. Two interesting components that are part of the gate driver are the current sensor (LTS 15-NP 00-114076) and the flyback diode (FT2000AG). The current sensor affected how precisely the current was measured which had an impact on how all of the methods performed. The range this sensor could measure in was ± 5A. The current sensors output is a voltage and the scaling to current is seen in (3.1) and used in Figure A.2.

$$I = (V + 2.52) \cdot \frac{15}{1.875} \tag{3.1}$$

The flyback diode prevents the voltage spike described in section 2.5 from damaging the components when the power supply is disconnected. It is placed with reverse polarity from the power supply and in parallel to the solenoid as seen in Figure A.1 where HS is high side gate driver and LS is low side gate driver. This means that the flyback diode is reverse biased and will not conduct any current while external voltage is applied. When the power supply is disconnected the flyback diode then shorts the circuit until all the magnetic energy in the solenoid is dissipated as heat in the circuit [Krantz, -]. A useful diode for this application is the Schottky diode which has a fast switch time and a low forward voltage drop usually between 0.15V and 0.45V instead of a voltage drop between 0.6V to 1.7V as for standard diodes [Teja, 2018].

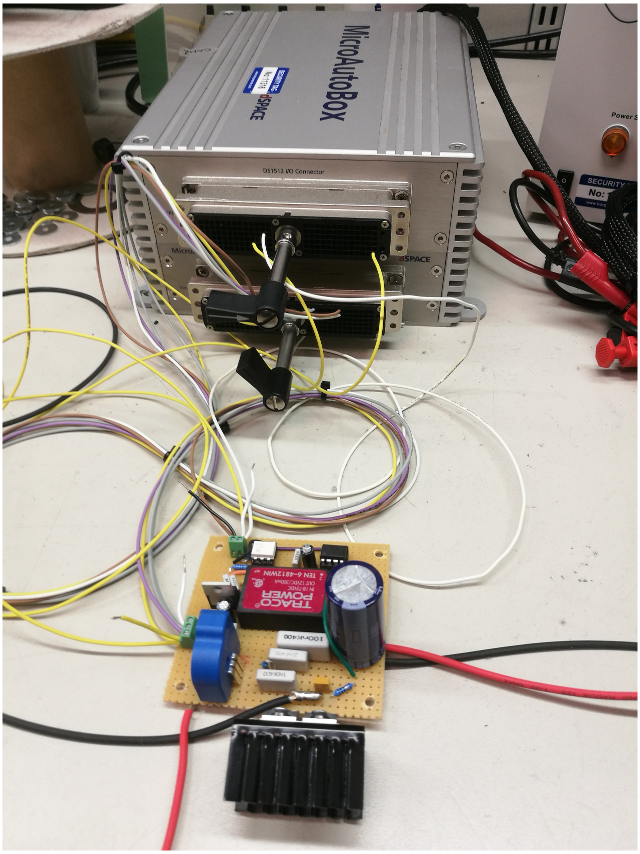

Figure 3.4 A picture of the MAB and the driver together with the connection between them.

dSpace software

The dSpace software contains Simulink blocks for real-time interface (RTI) and the MCAC block set which contains Analog-to-Digital Converter (ADC), PWM and PWM synchronized interrupt. ControlDesk is the software used for recording measurements and the layout used for the Simulink model FCmain can be seen in

Figure 3.5. The recordings were then saved into MATLAB files where the figures were made. Simulink was used as programming language for the MAB and all the modeling was done in Simulink which will be detailed in the next section. One big advantage with ControlDesk is that all the constants and some of the other block parameters can be set where an example is the threshold of the switch.

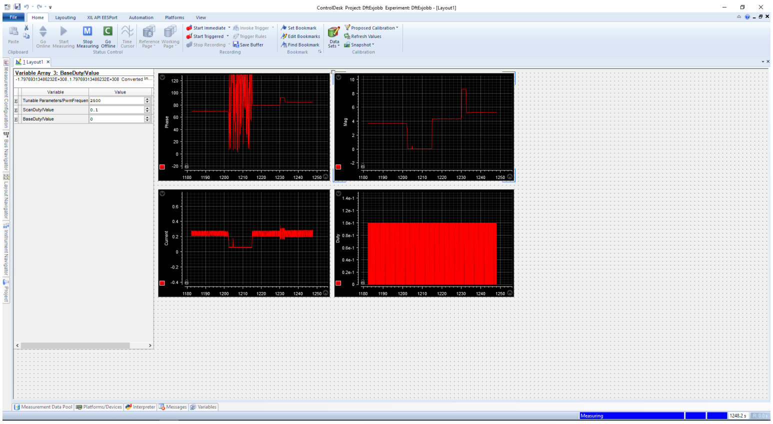

Figure 3.5 Monitoring using the software ControlDesk

3.2 Simulink models

The initialization file *Init.m* is run when the Simulink model is started, the init file is responsible for setting all the model parameters and contains the following code.

```
clear
close all
clc

PwmFrequency  = 2500;
SamplingTime = 0.1;
ScanFrequency = 100;
SamplingVectorSize = PwmFrequency * SamplingTime;

for i=1:1:(SamplingVectorSize)
    SinusDutyTable(i) = (sin(((1/PwmFrequency)*(i-1)) *
                         ScanFrequency*2*pi) + 1)*0.5;
end
```

In Figure A.2 the first layer of the model FCmain is shown which contains the PWM (AC_Motor_Generic_Commutation) and ADC (AC_Motor_ADC) block. The sample time of the model is set to 10000Hz while the PWM frequency is set to 2500Hz. The ADC block uses an integral filter to give a stable output. The way the filter works is that the ADC samples with a rate of 10MHz and then the average is calculated each PWM period. The AC_Motor_Setup block is necessary to make the ADC, PWM and interrupt (FC_Interrupt and AC_Motor_PWMSynchronous_Interrupt, referred to as PWM_interrupt) blocks work. The PWM_interrupt triggers the subsystem FCAndDutyCalc each PWM period at pulse mid. When the CosSum and SinSum (the FC) are ready FC_Interrupt triggers the ExtractPhaseMag subsystem where the phase and magnitude are extracted from the FC. The time from the first ADC sample to the result is around 100ms which is the maximum allowed time as stated in the introduction chapter. Figure A.3 shows the subsystem FCAndDutyCalc and consists of the the two subsystems FCCalc and DutyCalc and also the link between them. The figure also shows how the sums and sinus table are reset by SumsComplete. Figure A.4 shows the block in which the FC are calculated. The subsystem DutyCalc seen in Figure A.5 calculates the duty cycle. The subsystem ExtractPhaseMag which is trigged by the signal SumsComplete can be seen in Figure A.6. All the processing that is done to the phase (which is the output from the atan2 block) is to first convert it to degrees and then to get the value to represent the current lag compared to the voltage.

4

Results

A frequency sweep was conducted to determine the scan signal frequency for the phase and magnitude-based methods and the method used perform this sweep was FC. The PWM frequency for the sweep was set to 2500Hz. The voltage was set to 30V and the reason it was chosen to be 30V was because the solenoid was not rated to operate at higher voltages in combination with a high duty cycle. The amplitude of the scan signal was 10% duty cycle and both 0% and 10% base duty cycle was tested for every frequency in the sweep. The scan signal frequencies investigated were in the range of 10-150Hz. The result from the frequency sweep can be seen under the Frequency sweep section. Almost all of the measurement methods used the same configuration as the frequency sweep. The exceptions are time constant, current controller and FFT. Also a current in the holding-mode of 0.5A was needed to keep the spring compressed, this corresponds to 5% base duty cycle at 30V. There is also a section where possible optimizations are investigated by changing the parameters presented above.

In this chapter, position signal plots are presented for the investigated methods. These plots are intended to show how the position signal varies with the position. The position signals are presented as functions of time, where the actual position at a certain time interval is marked in the plots. For these plots the solenoid is placed in the stand as shown in Figure 3.2. The spikes between the position intervals is where the solenoid plunger is lifted to allow the next group of washers to be inserted to represent a new position.

4.1 Frequency sweep

This sections shows the results of the frequency sweep described in the theory chapter. To sweep through the frequencies the ScanFrequency parameter in the *Init.m* file was changed. The method that was used to perform the sweep was FC, to get a result for both the magnitude and the phase at the same time. The result for the frequencies investigated can be seen in Table 4.1 for the phase and in Table 4.2 for the magnitude. After performing this sweep it was decided that the phase-based methods will use a scan frequency of 100Hz. The magnitude-based methods will also use 100Hz. This is because the variance is very low so the difference between the 0mm position and 6mm position do not play as big role for this methods so its better to have only one frequency.

Freq	Phase 0mm	Phase 6mm	Diff	Var 0mm	Var 6mm
10Hz	47.4	40.4	7.0	0.07	0.01
20Hz	48.2	55.2	7.0	0.06	0.01
30Hz	49.8	61.7	11.9	0.07	0.01
40Hz	51.9	66.7	14.8	0.09	0.02
50Hz	54.5	71.3	16.8	0.08	0.03
60Hz	57.3	74.4	17.1	0.08	0.03
70Hz	60.2	77.5	17.3	0.09	0.03
80Hz	63.1	80.5	17.4	0.09	0.04
90Hz	66.1	83.4	17.3	0.10	0.05
100Hz	69.3	86.3	17.0	0.10	0.04
110Hz	72.1	89.0	16.9	0.13	0.05
120Hz	75.1	91.8	16.7	0.09	0.05
130Hz	77.7	94.1	16.4	0.09	0.06
140Hz	80.7	96.8	16.1	0.12	0.05
150Hz	84.2	100.1	15.9	0.11	0.06

Table 4.1 Phase shift and variance at plunger position 0mm and 6mm for different scan signal frequencies.

Freq	Mag 0mm	Mag 6mm	Diff	Var 0mm	Var 6mm
10Hz	9.3	22.9	13.6	$18 \cdot 10^{-4}$	$17 \cdot 10^{-4}$
20Hz	6.8	15.7	8.9	$8.94 \cdot 10^{-4}$	$8.97 \cdot 10^{-4}$
30Hz	5.8	12.0	6.2	$6.13 \cdot 10^{-4}$	$6.53 \cdot 10^{-4}$
40Hz	5.2	10.1	4.9	$6.78 \cdot 10^{-4}$	$6.31 \cdot 10^{-4}$
50Hz	4.8	8.7	3.9	$6.33 \cdot 10^{-4}$	$4.39 \cdot 10^{-4}$
60Hz	4.5	7.7	3.2	$4.81 \cdot 10^{-4}$	$4.60 \cdot 10^{-4}$
70Hz	4.2	6.9	2.7	$4.12 \cdot 10^{-4}$	$4.38 \cdot 10^{-4}$
80Hz	4.0	6.3	2.3	$4.11 \cdot 10^{-4}$	$4.24 \cdot 10^{-4}$
90Hz	3.8	5.9	2.1	$4.18 \cdot 10^{-4}$	$3.79 \cdot 10^{-4}$
100Hz	3.6	5.5	1.9	$3.06 \cdot 10^{-4}$	$4.31 \cdot 10^{-4}$
110Hz	3.5	5.1	1.6	$3.89 \cdot 10^{-4}$	$2.84 \cdot 10^{-4}$
120Hz	3.4	4.9	1.5	$2.97 \cdot 10^{-4}$	$3.52 \cdot 10^{-4}$
130Hz	3.4	4.6	1.2	$3.37 \cdot 10^{-4}$	$4.89 \cdot 10^{-4}$
140Hz	3.3	4.4	1.1	$3.25 \cdot 10^{-4}$	$4.28 \cdot 10^{-4}$
150Hz	3.1	4.2	1.0	$3.27 \cdot 10^{-4}$	$3.52 \cdot 10^{-4}$

Table 4.2 Magnitude and variance at plunger position 0mm and 6mm for different scan signal frequencies.

4.2 Resistance and inductance measurements

This section contains data from the experiments with the LCR meter. The LCR meter used a sinusoidal wave with amplitude 1.5V to perform the measurements. It was possible to configure the LCR meter to use different frequencies for the sinusoidal wave. In Table 4.3 the resistance, inductance and impedance of the solenoid for different frequencies at position 0mm are shown. In Figure 4.1 the resistance and reactance are plotted as functions of frequency at position 0mm.

In Table 4.4 the resistance, inductance and impedance of the solenoid for different frequencies at position 6mm are shown. In Figure 4.2 the resistance and reactance are plotted as functions of frequency at position 6mm.

Table 4.5 shows the resistance, inductance and impedance of the solenoid for different temperatures for measurement signal frequency 100Hz at position 0mm, in Table 4.6 the corresponding values at position 6mm are shown.

Frequency	Resistance	Inductance	Impedance	Arctan($\frac{\omega L}{R}$)
1Hz	5.0Ω	0.281H	5.3Ω	19.4°
10Hz	11.2Ω	0.198H	16.8Ω	48.0°
20Hz	18.5Ω	0.142H	25.7Ω	44.0°
50Hz	29.9Ω	0.0786H	38.7Ω	39.6°
100Hz	47.2Ω	0.0545H	58.3Ω	36.0°
1000Hz	101.7Ω	0.0122H	127.6Ω	37.0°
2500Hz	136.5Ω	0.00739H	179.0Ω	40.4°
10000Hz	207.4Ω	0.00461H	356.4Ω	54.4°
100000Hz	1180.8Ω	0.00266H	2050.3Ω	54.8°

Table 4.3 The solenoid resistance, inductance and impedance for different frequencies at plunger position 0mm.

Frequency	Resistance	Inductance	Impedance	Arctan($\frac{\omega L}{R}$)
1Hz	4.7Ω	0.0737H	4.7Ω	5.6°
10Hz	5.3Ω	0.0716H	5.9Ω	40.3°
20Hz	6.6Ω	0.0674H	10.8Ω	52.1°
50Hz	11.6Ω	0.0551H	20.8Ω	56.2°
100Hz	19.3Ω	0.0454H	34.4Ω	55.9°
1000Hz	83.2Ω	0.0132H	117.3Ω	44.9°
2500Hz	123.7Ω	0.00791H	175.3Ω	45.1°
10000Hz	204.7Ω	0.00470H	359.1Ω	55.3°
100000Hz	1217.7Ω	0.00268H	2077.9Ω	54.1°

Table 4.4 The solenoid resistance, inductance and impedance for different frequencies at plunger position 6mm.

Temperature	Resistance	Inductance	Impedance	Arctan($\frac{\omega L}{R}$)
-30°C	43.8Ω	0.0510H	54.2Ω	36.2°
-20°C	44.3Ω	0.0515H	54.9Ω	36.1°
-10°C	44.7Ω	0.0519H	55.4Ω	36.1°
0°C	45.4Ω	0.0528H	56.3Ω	36.2°
10°C	46.3Ω	0.0537H	57.3Ω	36.1°
20°C	47.3Ω	0.0547H	58.6Ω	36.0°
30°C	48.4Ω	0.0559H	59.9Ω	36.0°
40°C	49.3Ω	0.0568H	60.9Ω	35.9°
50°C	50.0Ω	0.0575H	61.7Ω	35.9°
60°C	51.0Ω	0.0588H	63.0Ω	35.9°
70°C	52.5Ω	0.0601H	64.7Ω	35.7°
80°C	53.8Ω	0.0616H	66.4Ω	35.7°
90°C	54.9Ω	0.0626H	67.6Ω	35.6°
100°C	56.4Ω	0.0643H	69.4Ω	35.6°

Table 4.5 Temperature measurements at plunger position 0mm with measurement frequency 100Hz.

Temperature	Resistance	Inductance	Impedance	Arctan($\frac{\omega L}{R}$)
-30°C	18.9Ω	0.0434H	33.2Ω	55.3°
-20°C	18.9Ω	0.0435H	33.3Ω	55.3°
-10°C	19.0Ω	0.0438H	33.4Ω	55.4°
0°C	19.1Ω	0.0442H	33.7Ω	55.5°
10°C	19.3Ω	0.0450H	34.2Ω	55.7°
20°C	19.5Ω	0.0456H	34.7Ω	55.8°
30°C	19.8Ω	0.0464H	35.2Ω	55.8°
40°C	20.0Ω	0.0470H	35.7Ω	55.9°
50°C	20.2Ω	0.0475H	36.0Ω	55.9°
60°C	20.3Ω	0.0480H	36.4Ω	56.1°
70°C	20.5Ω	0.0484H	36.7Ω	56.0°
80°C	20.6Ω	0.0488H	37.0Ω	56.1°
90°C	20.8Ω	0.0495H	37.4Ω	56.2°
100°C	21.0Ω	0.0503H	37.9Ω	56.4°

Table 4.6 Temperature measurements at plunger position 6mm with measurement frequency 100Hz.

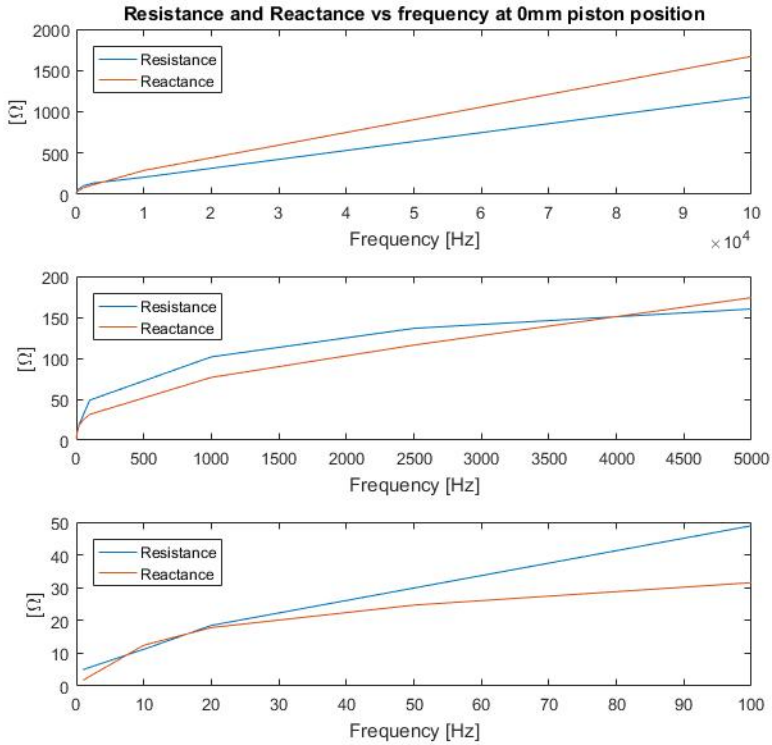

Figure 4.1 This figure shows the frequency dependency of resistance and reactance at plunger position 0mm.

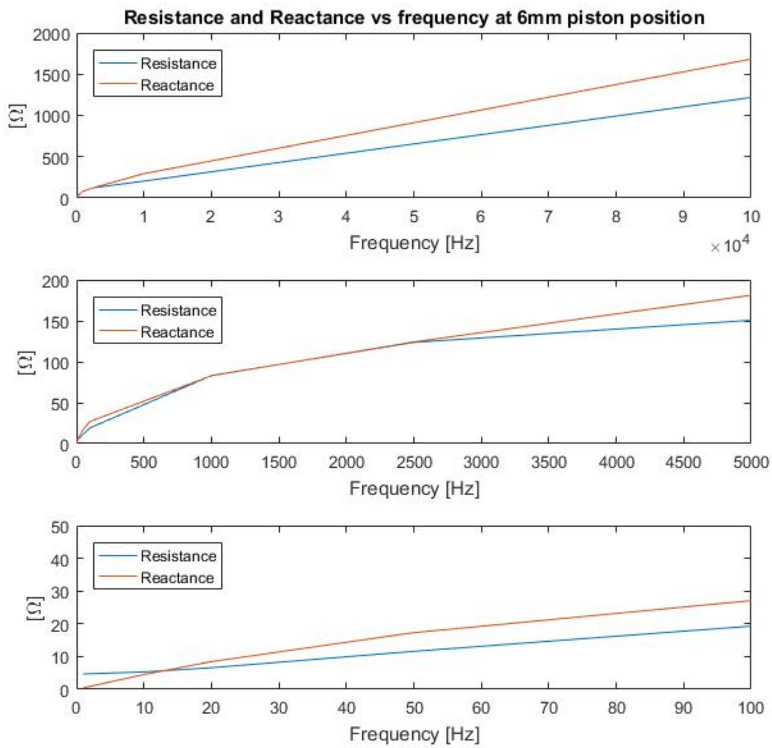

Figure 4.2 This figure shows the frequency dependency of resistance and reactance at plunger position 6mm.

4.3 Time measurements

In Table 4.7 the time for calculating the result for the different methods is shown. This measurement was done in MATLAB using the *tic* and *toc* commands. As seen the covariance and the convolution are extremely slow so no further experiments with these methods were done. The time in Table 4.7 is the time taken for one million calculations, the average time is the time taken for one calculation. All the calculations were made with 100ms as sample time and 2500Hz PWM frequency (2560Hz for FFT) with the exception for time constant and the current control methods since their fundamentals are completely different to the other methods. There is no result for the method Time constant - Least-squares estimation, this is because it was not possible to achieve the required sample rate needed for this method. The start option *singleCompThread* was used to limit MATLAB to a single computational thread. This was done because the CPU in the MAB does only have one core.

Method	Time	Average Time
Current amplitude	13s	$1.3 \cdot 10^{-5}$s
Convolution	54s	$5.4 \cdot 10^{-5}$s
Covariance	81s	$8.1 \cdot 10^{-5}$s
Current control - Period	0.01s	$0.001 \cdot 10^{-5}$s
Fourier coefficients	3s	$0.3 \cdot 10^{-5}$s
Current control - Least squares	37s	$3.7 \cdot 10^{-5}$s
Fast Fourier transform	8s	$0.8 \cdot 10^{-5}$s
Current integration	32s	$3.2 \cdot 10^{-5}$s
Time constant - Period	0.04s	$0.004 \cdot 10^{-5}$s
Zero crossing	20s	$2 \cdot 10^{-5}$s

Table 4.7 Calculation time.

4.4 Phase-based methods

This section contains results from zero crossing and FFT.

Zero crossing

Three position signal plots were made for this method, they can be seen in Figure 4.3 where no base duty cycle was used, Figure 4.4 with 10% base duty cycle and Figure 4.5 with 30% base duty cycle.

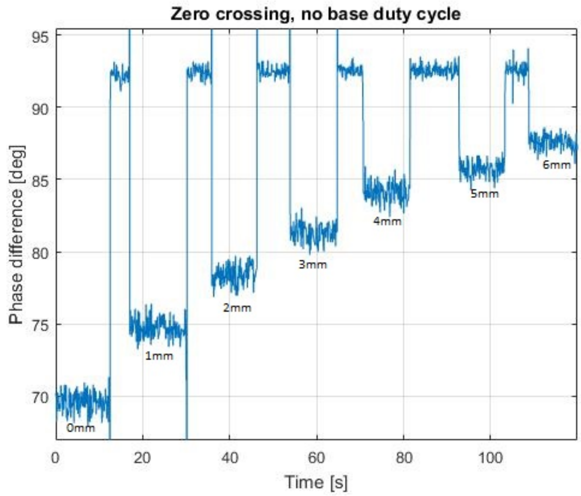

Figure 4.3 Position signal at different positions using zero crossing. PWM frequency 2500Hz, scan signal frequency 100Hz, scan signal percentage 10, base duty percentage 0, temperature 22°C. The sampling time was set to 100ms.

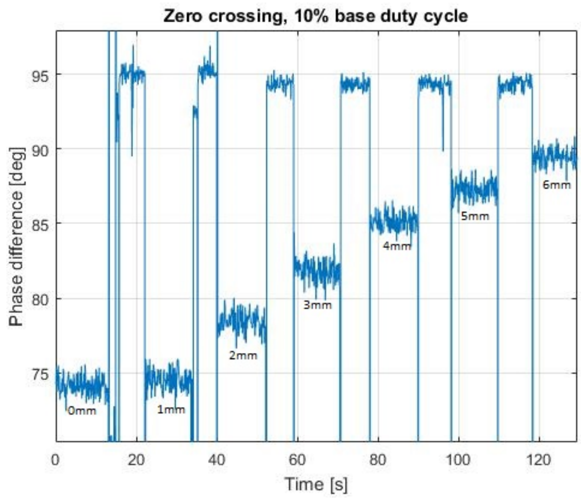

Figure 4.4 Position signal at different positions using zero crossing. PWM frequency 2500Hz, scan signal frequency 100Hz, scan signal percentage 10, base duty percentage 10, temperature 22°C. The sampling time was set to 100ms.

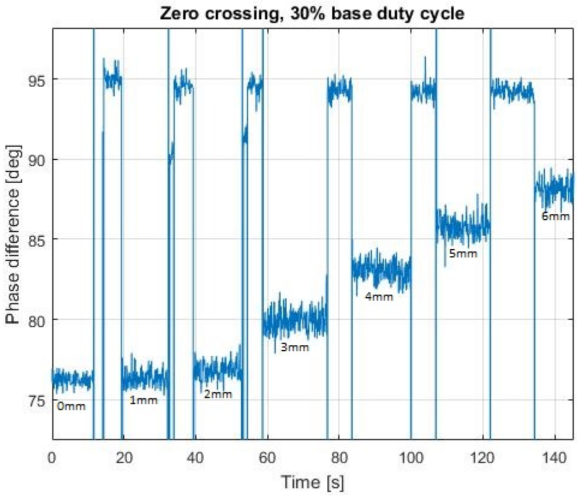

Figure 4.5 Position signal at different positions using zero crossing. PWM frequency 2500Hz, scan signal frequency 100Hz, scan signal percentage 10, base duty percentage 30, temperature 22°C. The sampling time was set to 100ms.

Fast Fourier transform

Since the FFT algorithms assumes that the length of the vector is a power of 2, the chosen length was 256 samples. The performance of this method can be seen in the position signal plots in Figure 4.6 with no base duty cycle, Figure 4.7 with 0.05 base duty cycle, Figure 4.8 with 0.1 base duty cycle and Figure 4.9 with 0.3 base duty cycle. To investigate the temperature dependency of this method, a series of measurements were conducted with 0.05 base duty cycle, 0.1 scan duty cycle and position 0mm, this can be seen in Table 4.8.

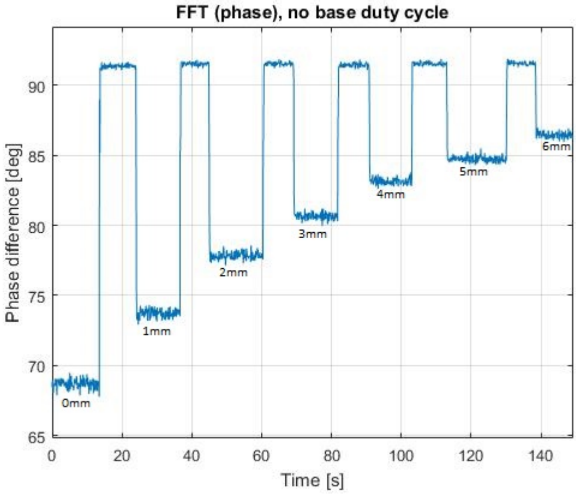

Figure 4.6 Position signal at different positions using FFT phase calculation. PWM frequency 2560Hz, scan signal frequency 100Hz, scan signal percentage 10, base duty percentage 0, temperature 22°C. The sampling time was set to 100ms.

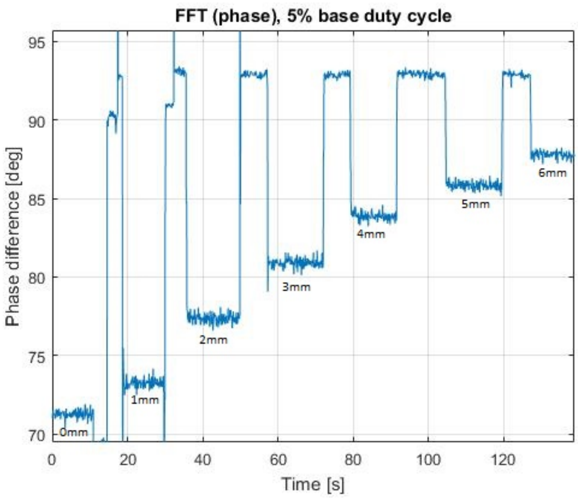

Figure 4.7 Position signal at different positions using FFT phase calculation. PWM frequency 2560Hz, scan signal frequency 100Hz, scan signal percentage 10, base duty percentage 5, temperature 22°C. The sampling time was set to 100ms.

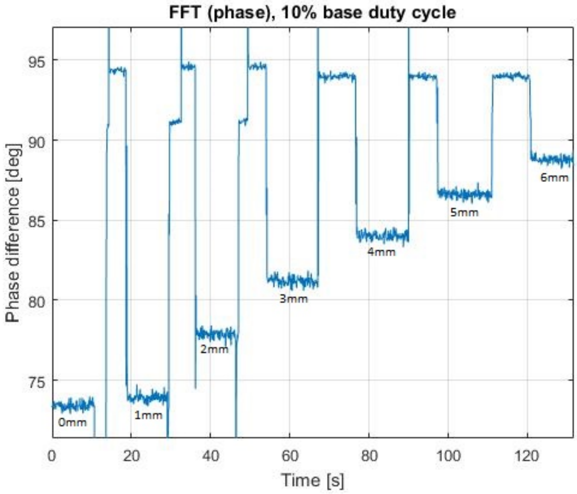

Figure 4.8 Position signal at different positions using FFT phase calculation. PWM frequency 2560Hz, scan signal frequency 100Hz, scan signal percentage 10, base duty percentage 10, temperature 22°C. The sampling time was set to 100ms.

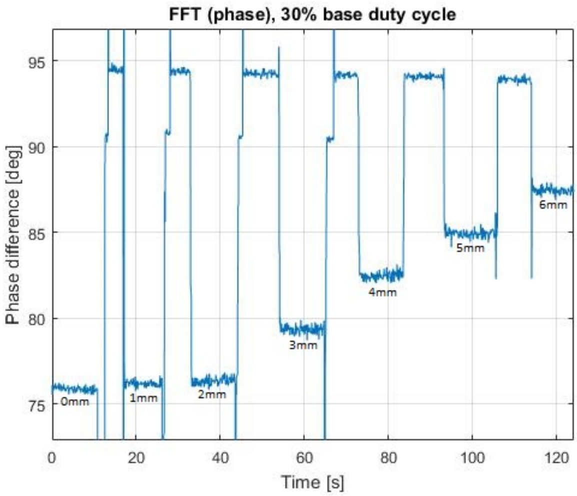

Figure 4.9 Position signal at different positions using FFT phase calculation. PWM frequency 2560Hz, scan signal frequency 100Hz, scan signal percentage 10, base duty percentage 30, temperature 22°C. The sampling time was set to 100ms.

Temperature	Phase
$-40°C$	71.6°
$-30°C$	71.5°
$-20°C$	72.2°
$-10°C$	71.3°
0°C	72.0°
10°C	71.2°
20°C	71.7°
30°C	71.1°
40°C	71.5°
50°C	71.2°
60°C	71.4°
70°C	71.3°
80°C	71.3°
90°C	71.2°
100°C	71.1°
110°C	70.9°
120°C	71.0°
130°C	70.9°
140°C	71.0°

Table 4.8 Phase difference for different temperature using FFT. PWM frequency 2560Hz, scan signal frequency 100Hz, 0.05 base duty cycle, 0.1 scan duty cycle, at position 0mm. The sampling time was set to 100ms.

Convolution

As seen in Table 4.7 the estimated calculation time for Convolution was very long. Because of this no position signal experiments were conducted for this method.

Covariance

As seen in Table 4.7 the estimated calculation time for Covariance was very long. Because of this no position signal experiments were conducted for this method.

4.5 Magnitude-based methods

This section contains results from current amplitude, current integration and current control.

Current amplitude

Since the current integral method is a more robust method that builds on the same principle as current amplitude, only a few measurements were conducted for this method. The position signal results are shown in Figure 4.10 with no base, Figure 4.11 with 0.1 base duty cycle and Figure 4.12 with 0.3 base duty cycle.

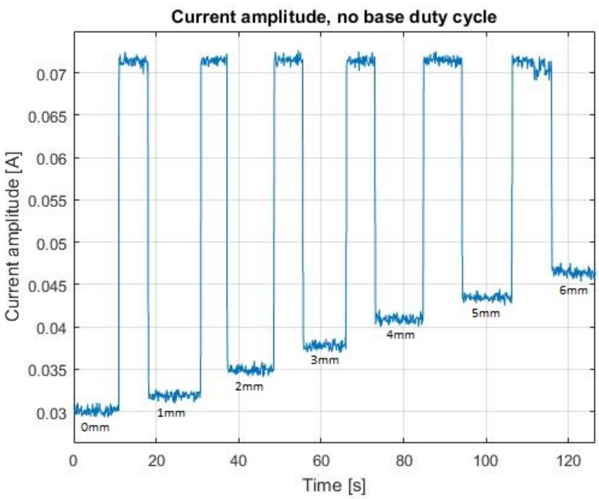

Figure 4.10 Position signal at different positions using current amplitude. PWM frequency 2500Hz, scan signal frequency 100Hz, scan signal percentage 10, base duty percentage 0, temperature 22°C. The sampling time was set to 100ms.

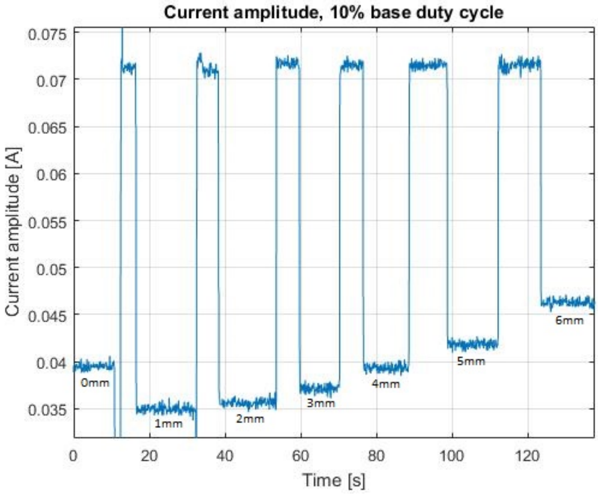

Figure 4.11 Position signal at different positions using current amplitude. PWM frequency 2500Hz, scan signal frequency 100Hz, scan signal percentage 10, base duty percentage 10, temperature 22°C. The sampling time was set to 100ms.

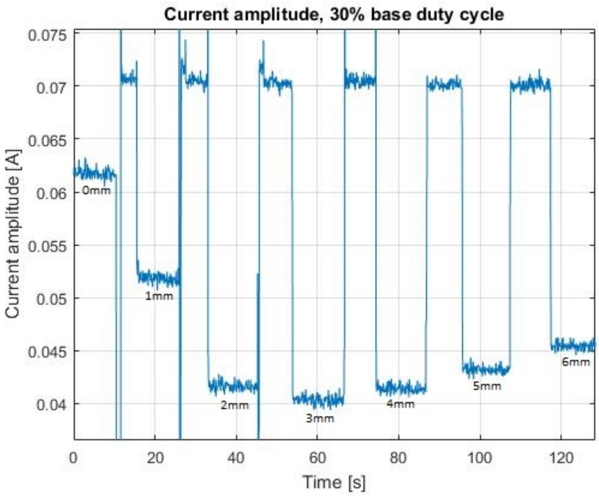

Figure 4.12 Position signal at different positions using current amplitude. PWM frequency 2500Hz, scan signal frequency 100Hz, scan signal percentage 10, base duty percentage 30, temperature 22°C. The sampling time was set to 100ms.

Current integration

The position signal at 100Hz is shown in Figure 4.13 with no base duty cycle, Figure 4.14 with 0.1 base duty cycle and Figure 4.15 with 0.3 base duty cycle.

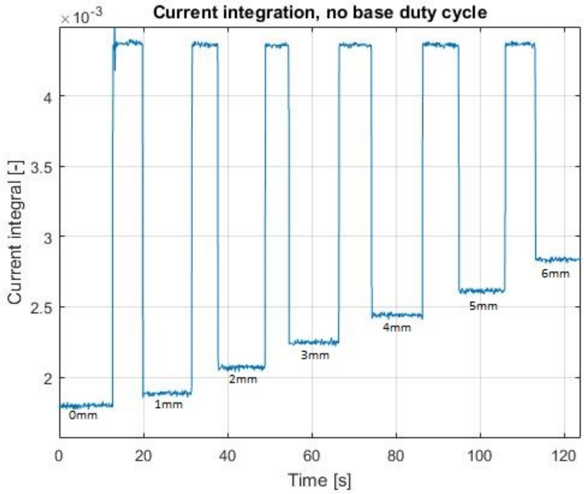

Figure 4.13 Position signal at different positions using current integration. PWM frequency 2500Hz, scan signal frequency 100Hz, scan signal percentage 10, base duty percentage 0, temperature 22°C. The sampling time was set to 100ms.

To investigate the temperature dependency, a series of measurements for this method were made for no base duty cycle, 0.1 scan duty cycle at position of 0mm, this can be seen in Table 4.9.

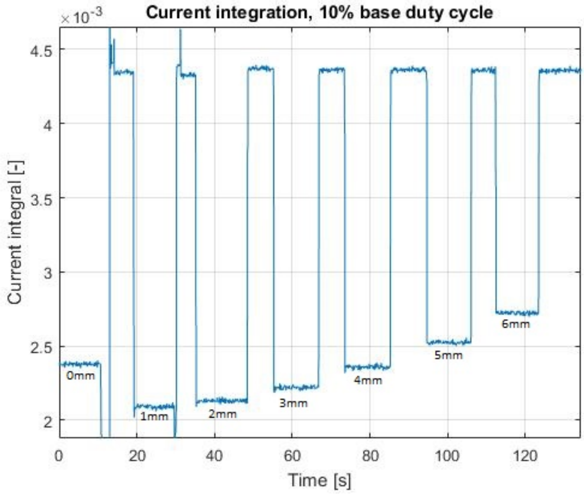

Figure 4.14 Position signal at different positions using current integration. PWM frequency 2500Hz, scan signal frequency 100Hz, scan signal percentage 10, base duty percentage 10, temperature 22°C. The sampling time was set to 100ms.

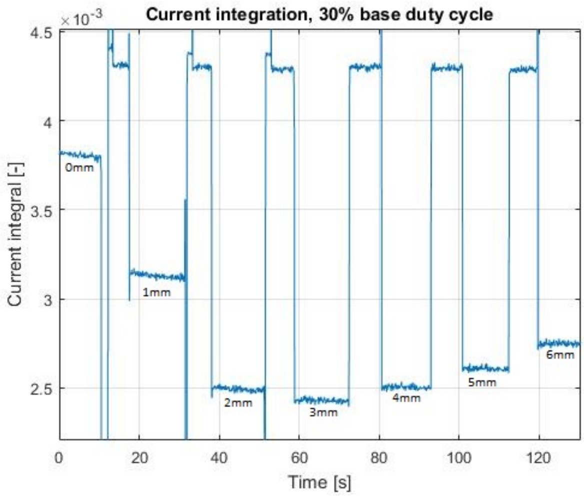

Figure 4.15 Position signal at different positions using current integration. PWM frequency 2500Hz, scan signal frequency 100Hz, scan signal percentage 10, base duty percentage 30, temperature 22 °C. The sampling time was set to 100ms.

Temperature	Integral
$-40°C$	$1.89 \cdot 10^{-3}$
$-30°C$	$2.02 \cdot 10^{-3}$
$-20°C$	$1.95 \cdot 10^{-3}$
$-10°C$	$1.97 \cdot 10^{-3}$
$0°C$	$1.87 \cdot 10^{-3}$
$10°C$	$1.88 \cdot 10^{-3}$
$20°C$	$1.78 \cdot 10^{-3}$
$30°C$	$1.79 \cdot 10^{-3}$
$40°C$	$1.74 \cdot 10^{-3}$
$50°C$	$1.74 \cdot 10^{-3}$
$60°C$	$1.69 \cdot 10^{-3}$
$70°C$	$1.68 \cdot 10^{-3}$
$80°C$	$1.62 \cdot 10^{-3}$
$90°C$	$1.61 \cdot 10^{-3}$
$100°C$	$1.56 \cdot 10^{-3}$
$110°C$	$1.55 \cdot 10^{-3}$
$120°C$	$1.51 \cdot 10^{-3}$
$130°C$	$1.51 \cdot 10^{-3}$
$140°C$	$1.47 \cdot 10^{-3}$

Table 4.9 Integral values for different temperature using integration with PWM frequency 2560Hz, scan signal frequency 100Hz, no base duty cycle, 0.1 scan duty cycle, at position 0mm. The sampling time was set to 100ms.

Current control

Current control - Period The position signal for Current control (period) is shown in Figure 4.16 without current offset and Figure 4.17 with current offset 0.5A.

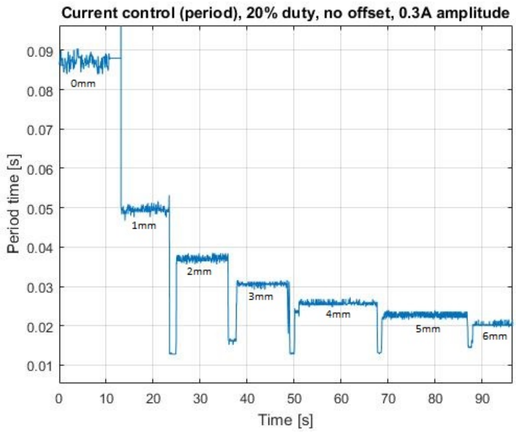

Figure 4.16 Position signal at different positions using current control (period). PWM frequency 2500Hz, duty cycle 20%, no current offset, current amplitude 0.3A, temperature 22°C.

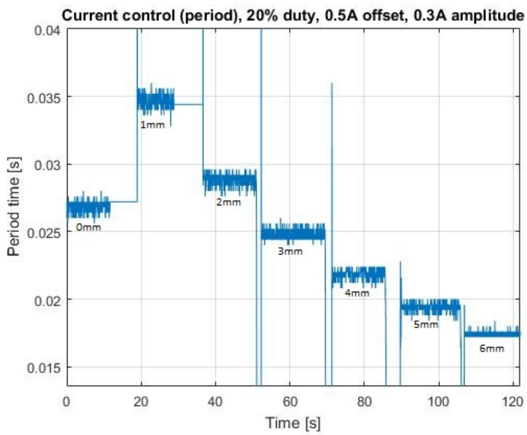

Figure 4.17 Position signal at different positions using current control (period). PWM frequency 2500Hz, duty cycle 20%, 0.5A current offset, current amplitude 0.3A, temperature 22°C.

Current control - Least-squares estimation The position signal for Current control (LS) is shown in Figure 4.18 without current offset and Figure 4.19 with 0.5A current offset.

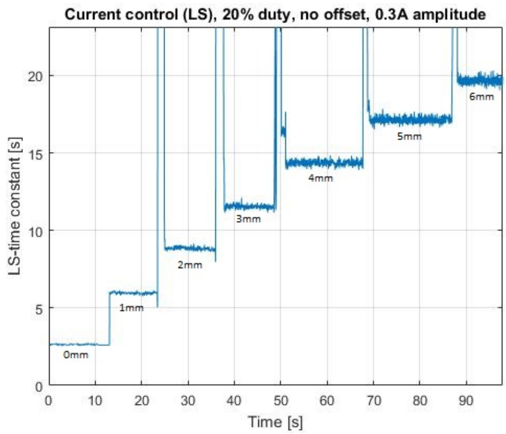

Figure 4.18 Position signal at different positions using current control LS. PWM frequency 2500Hz, duty cycle 20%, no current offset, current amplitude 0.3A, temperature 22°C.

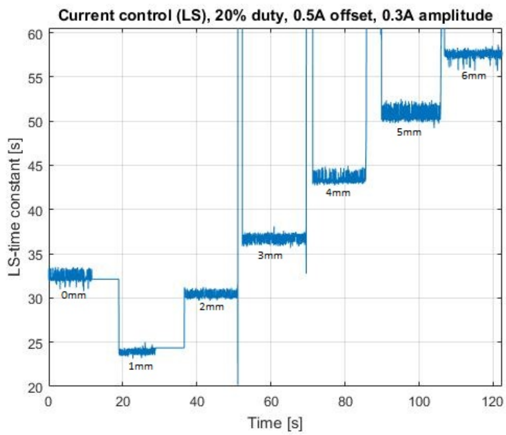

Figure 4.19 Position signal at different positions using current control LS. PWM frequency 2500Hz, duty cycle 20%, 0.5A current offset, current amplitude 0.3A, temperature 22°C.

4.6 Time constant

There is no result to show from this method for either of the two variations. The time constant period measurements that was done for this method was noisy and the position levels were too indistinct to provide any useful information. As stated under time measurements time constant LS was never doable so there were no results from this method to show.

4.7 Fourier coefficients

The PWM frequency could be set to 2500Hz since this method did not require 2^n samples for reduced time complexity as with FFT. Figure 4.20 and Figure 4.21 shows the phase result with 0% respective 5% base duty cycle while Figure 4.23 and Figure 4.24 shows the magnitude result for the same duty cycle. Figure 4.22 and Figure 4.25 shows measurement for very high current, base duty cycle of 90%.

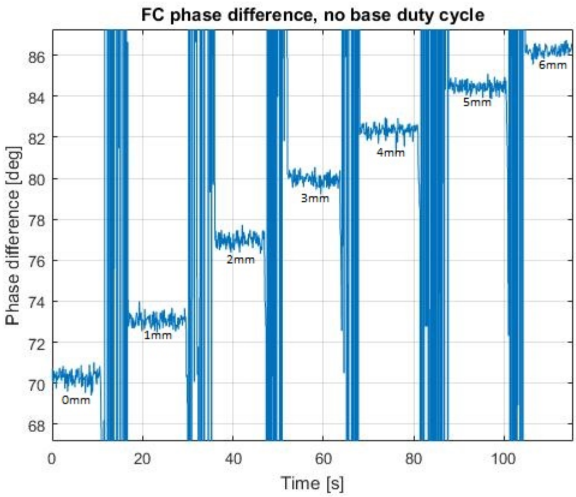

Figure 4.20 Position signal at different positions using phase response from FC. PWM frequency 2500Hz, scan signal frequency 100Hz, scan signal percentage 10, base duty percentage 0, temperature 22°C. The sampling time was set to 100ms.

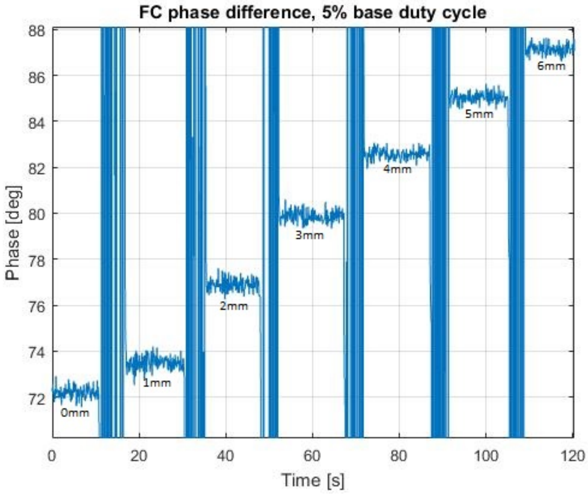

Figure 4.21 Position signal at different positions using phase response from FC. PWM frequency 2500Hz, scan signal frequency 100Hz, scan signal percentage 10, base duty percentage 5, temperature 22°C. The sampling time was set to 100ms.

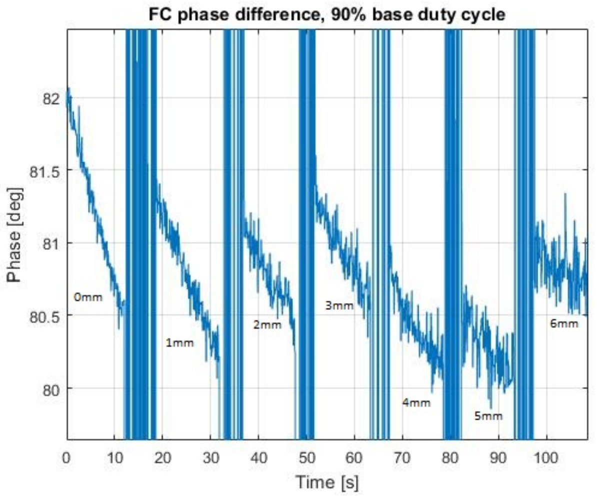

Figure 4.22 Position signal at different positions using phase response from FC. PWM frequency 2500Hz, scan signal frequency 100Hz, scan signal percentage 10, base duty percentage 90, temperature 22°C. The sampling time was set to 100ms.

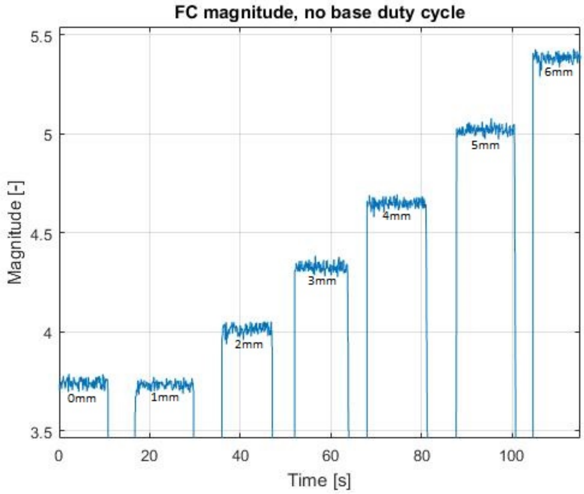

Figure 4.23 Position signal at different positions using magnitude response from FC. PWM frequency 2500Hz, scan signal frequency 100Hz, scan signal percentage 10, base duty percentage 0, temperature 22°C. The sampling time was set to 100ms.

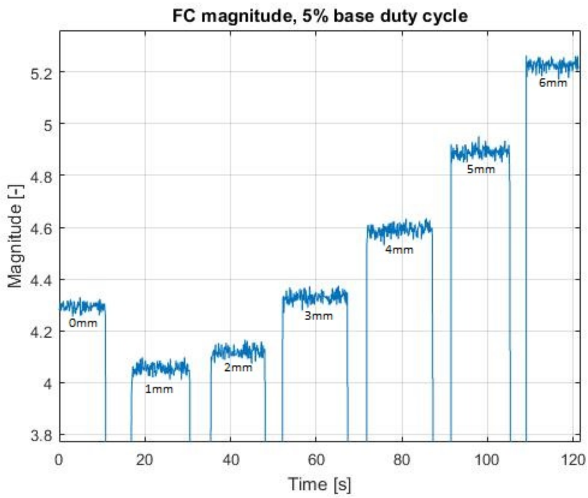

Figure 4.24 Position signal at different positions using magnitude response from FC. PWM frequency 2500Hz, scan signal frequency 100Hz, scan signal percentage 10, base duty percentage 5, temperature 22°C. The sampling time was set to 100ms.

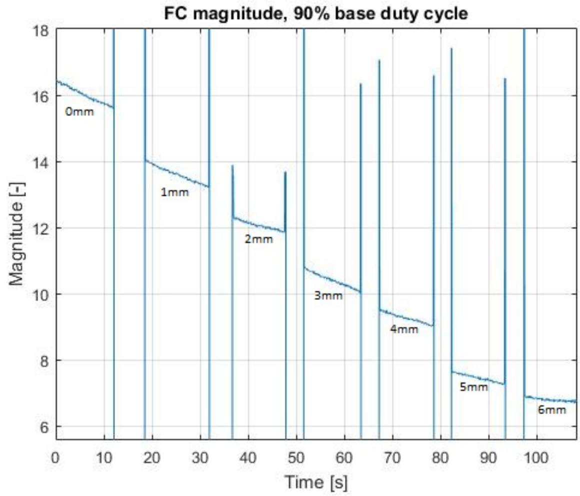

Figure 4.25 Position signal at different positions using magnitude response from FC. PWM frequency 2500Hz, scan signal frequency 100Hz, scan signal percentage 10, base duty percentage 90, temperature 22°C. The sampling time was set to 100ms.

4.8 Optimization

This section contains optimization for the method that performed the best, which was FC. It will show results from changing the voltage level, measurement time and amplitude of the sinusoidal scan signal. This section is divided in two sections, one is for optimization of the phase measurements and the other is for optimization of the magnitude measurements. Since the voltage of the battery can vary, experiments were performed for this method to investigate the impact of voltage variations. How the phase depends on the voltage can be seen in Figure 4.26 at plunger position 0mm and in Figure 4.27 at plunger position 6mm. How the magnitude depends on the voltage can be seen in Figure 4.28 at plunger position 0mm and in Figure 4.29 at plunger position 6mm. The effect of lowering the measurement time can be seen in Figure 4.30 where the measurement time is 50ms, Figure 4.31 where the measurement time is 20ms and Figure 4.32 where the measurement time is 10ms. Measurements from lowering the scan signal amplitude can be seen in Figure 4.33 where the amplitude is 7%, Figure 4.34 where the amplitude is 4% and Figure 4.35 where the amplitude is 1%.

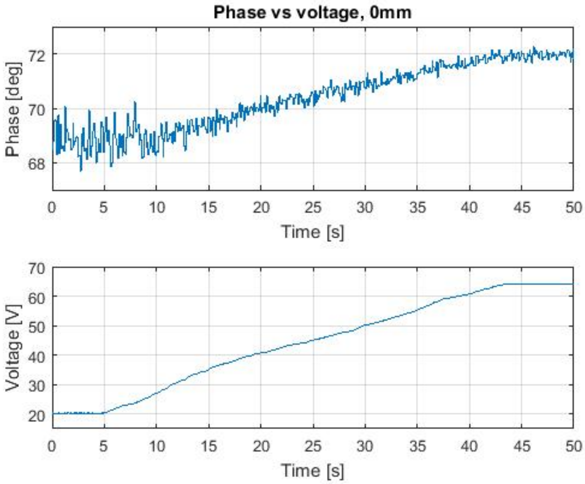

Figure 4.26 Voltage dependency for phase difference at 0mm calculated using FC. PWM frequency 2500Hz, scan signal frequency 100Hz, scan signal percentage 10, base duty percentage 0, temperature 22°C. The sampling time was set to 100ms.

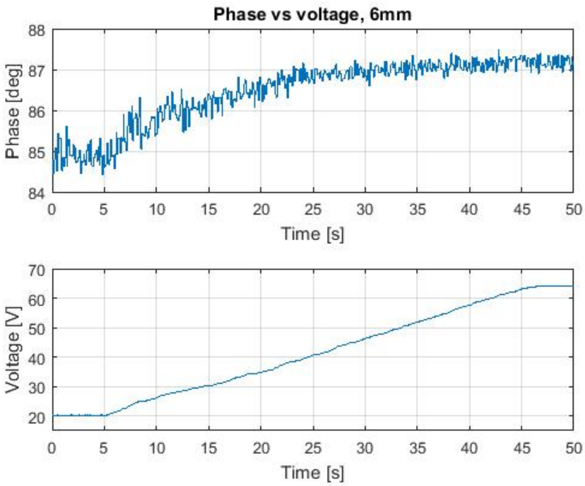

Figure 4.27 Voltage dependency for phase difference at 6mm calculated using FC. PWM frequency 2500Hz, scan signal frequency 100Hz, scan signal percentage 10, base duty percentage 0, temperature 22°C. The sampling time was set to 100ms.

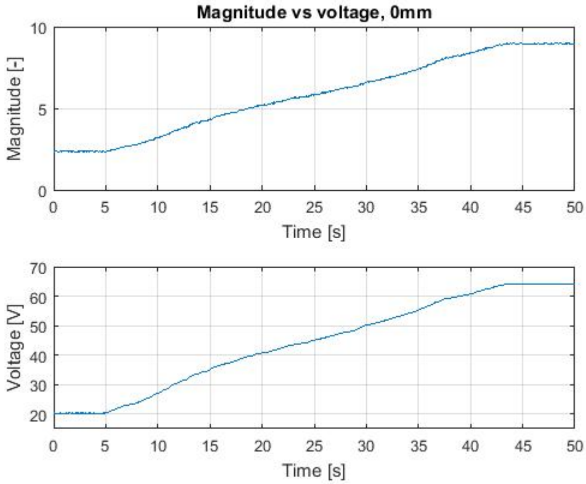

Figure 4.28 Voltage dependency for magnitude difference at 0mm calculated using FC. PWM frequency 2500Hz, scan signal frequency 100Hz, scan signal percentage 10, base duty percentage 0, temperature 22°C. The sampling time was set to 100ms.

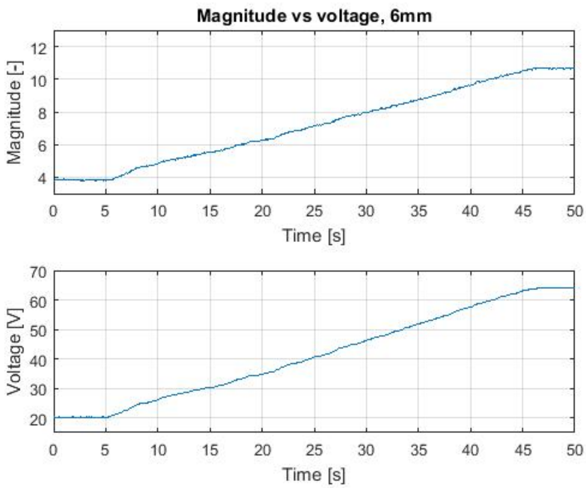

Figure 4.29 Voltage dependency for magnitude difference at 6mm calculated using FC. PWM frequency 2500Hz, scan signal frequency 100Hz, scan signal percentage 10, base duty percentage 0, temperature 22°C. The sampling time was set to 100ms.

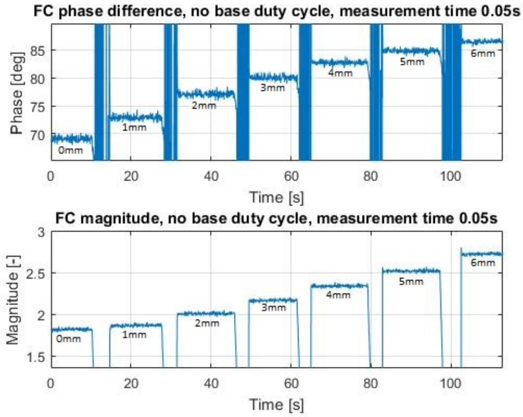

Figure 4.30 Optimization of measurement time using FC. PWM frequency 2500Hz, scan signal frequency 100Hz, scan signal percentage 10, base duty percentage 0, temperature 22°C. The sampling time was set to 50ms.

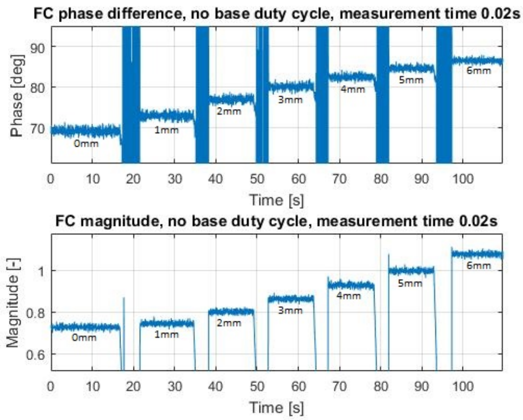

Figure 4.31 Optimization of measurement time using FC. PWM frequency 2500Hz, scan signal frequency 100Hz, scan signal percentage 10, base duty percentage 0, temperature 22°C. The sampling time was set to 20ms.

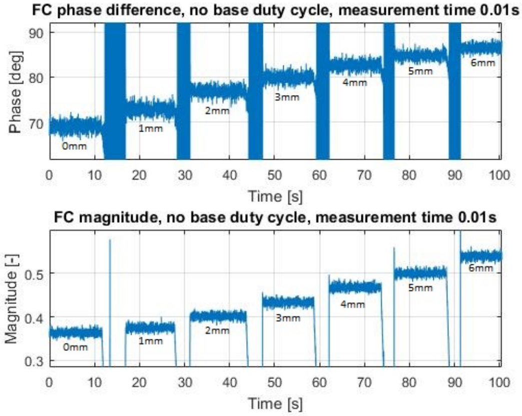

Figure 4.32 Optimization of measurement time using FC. PWM frequency 2500Hz, scan signal frequency 100Hz, scan signal percentage 10, base duty percentage 0, temperature 22°C. The sampling time was set to 10ms.

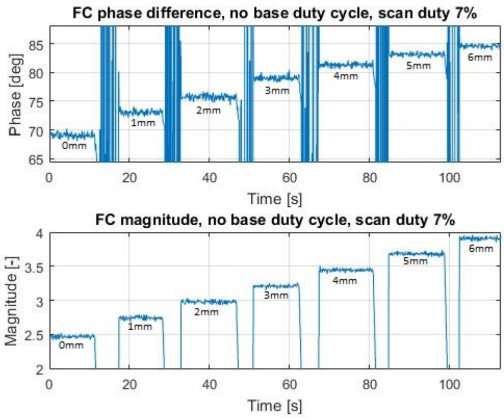

Figure 4.33 Optimization of the amplitude of the sinusoidal scan signal using FC. PWM frequency 2500Hz, scan signal frequency 100Hz, scan signal percentage 7, base duty percentage 0, temperature 22°C. The sampling time was set to 100ms.

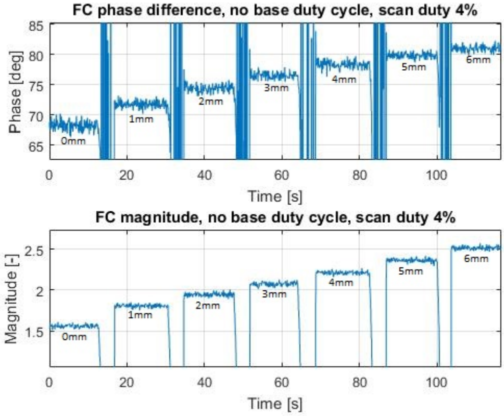

Figure 4.34 Optimization of the amplitude of the sinusoidal scan signal using FC. PWM frequency 2500Hz, scan signal frequency 100Hz, scan signal percentage 4, base duty percentage 0, temperature 22°C. The sampling time was set to 100ms.

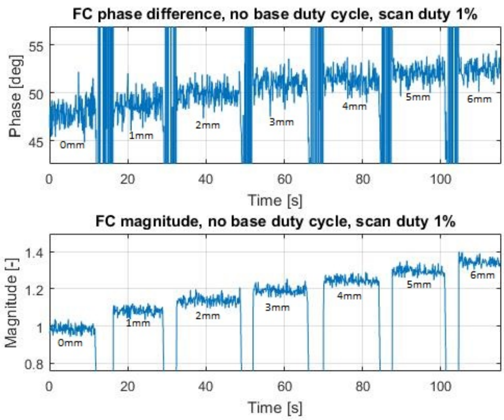

Figure 4.35 Optimization of the amplitude of the sinusoidal scan signal using FC. PWM frequency 2500Hz, scan signal frequency 100Hz, scan signal percentage 1, base duty percentage 0, temperature 22°C. The sampling time was set to 100ms.

5

Discussion

In this chapter the result of the different methods, some flaws in the time measurement and lastly some deeper analysis of the behaviour of the solenoid will be discussed. Due to time constraint the statements about temperature results from FFT and integration methods were only based at position 0mm which was the only temperature measurement for methods that was done. The same goes for the temperature and frequency measurement with the LCR meter but for both 0mm and 6mm.

5.1 Phase-based methods

In this section the different phase measurement methods are discussed, starting with zero crossing followed by FFT and convolution. The main advantage phase measurement had was the monotonic position levels in the holding-mode which can be seen for FFT in Figure 4.7. Other advantages were that they were less affected by varying supply voltage and temperature. The disadvantage of the phase-based method is that the variance is higher compared to the magnitude-based methods. Reflecting back on the scan signal frequency selection it can be seen from the result of the frequency sweep seen in Table 4.1 that 80Hz is better than 100Hz both in terms of variance and difference between 0mm and 6mm. However the difference is quite small and a decision was still made to use 100Hz.

Zero crossing

Zero crossing was a slower method than FFT and in Figure 4.3 and Figure 4.6 it can also be seen that zero crossing had higher variance than FFT. The implementation of Zero crossing only used two samples for the linear interpolation, which makes this method potentially bad at noise handling. Taking these disadvantages into consideration no further investigation of this method was made.

Fast Fourier transform

From the above statement this method is faster and has less variance than the zero crossing method which can be seen comparing Figure 4.6 and Figure 4.3. Since the position signal is monotonic in the holding-mode and because of the low calculation time, this method is potentially the best one.

Convolution

The time to calculate convolution is very long as seen in Table 4.7. Because of the very long calculation time it was not further investigated.

Covariance

As seen in Table 4.7 this was the slowest method and no further measurements were done using this method.

5.2 Magnitude-based methods

In this section the different magnitude-based measurement methods are discussed, starting with amplitude followed by integration and current control. The main advantage magnitude measurement had, was the low variance in the position signal which can for example be seen in Figure 4.13. The magnitude-based methods except current control also used 100Hz as a scan signal frequency. This is because the variance is very low so the difference between the 0mm position and 6mm position do not play as big role for this methods so its better to have only one frequency.

Current amplitude

When comparing Figure 4.10, Figure 4.11 and Figure 4.12 to Figure 4.13, Figure 4.14 and Figure 4.15 it is seen that integration method outperformed the amplitude method in terms of distinct position levels. In a noisy environment the variance is going to be even higher and then it will be difficult to distinguish the different position levels using this method. For a noisy method like this it could have been a good idea to try another frequency like 10Hz since the variance is much higher than for the integral method. Table 4.7 shows that this was faster than the integral method, the integral was calculated while new data was gathered which is stated in chapter 3, which makes it hard to compare the calculation time.

Current integration

This method was best in terms of most distinct position levels without a base duty cycle. The problem was when a base duty cycle was used as seen in Figure 4.13, Figure 4.14 and Figure 4.15 where the position signal vs. position is no longer monotonic. From Table 4.9 it is seen that this method is heavily temperature dependent.

Current control

The period variant of this method was noisier than the LS variant since it only used two measurement points which can be seen when comparing Figure 4.16 to Figure 4.18. This makes the period variant really fast compared to the LS variant which used all points on the downward slope for the LS estimation. The time difference can be seen in Table 4.7. For high current the same non-monotonic behaviour as for the other impedance magnitude-based methods is seen. This can be seen in the position signal plots: Figure 4.17 and Figure 4.19. Since this was the last method that was implemented, there was no time to perform as many different measurements as there were for FFT and integration.

5.3 Time constant

The downfall of the period variant was presumably that measuring only two points of the current leads to a very noisy signal. An attempt was made to filter it by calculating the mean or median of several measurements, however this had limited impact and it also slowed down the method. From Table 4.7 this method is by far the fastest, which was expected since it computes a position signal result for every PWM pulse. Since the period variant was so noisy the second variant LS, was made to reduce the noise but this did not work at all. The reason why it did not work was because the hardware could not handle such high sample rate this method required.

5.4 Fourier coefficients

FC provides the same information as FFT, but requires less computational power. When comparing the FC magnitude result to the current integration method it is seen that they are very similar. This together with its fast calculation time and its continuous calculations makes it the best method. As seen in the result there was no temperature plots of FC, this is because the similarity with the integration and FFT methods which already had those measurements done. There are two extra figures (Figure 4.22 and Figure 4.25) that shows the phase and magnitude with a base duty cycle of 90%. From these figures it is seen that the phase is around 81° for all positions while the magnitude has shifted and all the positions are distinguishable but the position of 0mm now have the highest magnitude while position of 6mm have the lowest. From Figure 4.26 and Figure 4.27 the dependency of supply voltage using phase measurement is shown. Figure 4.28 and Figure 4.29 shows the same dependency but for the magnitude. From this it is seen that the phase measurement is not affected as much as the magnitude measurement by varying voltage levels. This was anticipated since the amplitude was higher for higher voltage which increased the value of the magnitude. An attempt to optimize this method with lower sampling time can be seen in Figure 4.30, Figure 4.31 and Figure 4.32 for phase, where the position levels are distinct for times down to 50ms. The same figures but for for magnitude and can be seen that the position levels are distinct for times down to 20ms. An optimization attempt with lower scan signal amplitude is shown in Figure 4.33, Figure 4.34 and Figure 4.35 it is seen that the position levels can be distinguished down to the scan duty cycle 7% for phase and 4% for magnitude.

5.5 Time measurement

The goal of the time measurement was to see which method that performed fastest on the MAB, but there was no simple way of testing this. One way to measure the performance in terms of time was to count the amount of assembly instructions the program used, this is no simple task and therefore another approach was taken. The used approach was to simulate the measurements in MATLAB and there measure the time it took to do the calculations. Because of this approach the time measurement does not give a perfect estimation of how the methods will perform on the MAB, but it could still be used as an indicator for the time complexity of the methods.

5.6 Resistance and inductance

As explained in the inductance section in the theory chapter the inductance should be highest at plunger position 0mm. This appears to be also be the case when analyzing the measurements with the LCR meter which can be seen in Table 4.3 and Table 4.4, at least for scan signal frequencies lower than 1kHz. If only the inductance was dependent on the plunger position the phase difference between the current and the voltage would be greatest at plunger position 0mm. When looking at the position signal plots for the phase-based methods it can clearly be seen that this is not the case. This is because the relative change of resistance is greater than the relative change of inductance, at least for a scan frequency of 100Hz.

In Table 4.8 it can be seen that phase measurements was almost temperature independent which means that the relation between the resistance and inductance change very little with temperature.

Theoretically the phase difference should never exceed 90° since this implies negative resistance, but when the plunger is completely removed the phase difference is more than 90°. The reason for this is expected to be that the PWM frequency is insufficient to create a proper sinusoidal scan signal wave. Looking at Table 4.1 the phase increases as the scan frequency increases which implies it could be the insufficient PWM frequency that is causing this behaviour.

When comparing the measurements from the LCR meter (Table 4.3, Table 4.4) to the frequency sweep (Table 4.1) it is seen that the calculated phase difference with low scan signal frequency match quite well. However at scan signal 100Hz the values from the LCR meter and what is measured in the sweep differ much. This again implies that the PWM frequency is sufficient to create a good sinusoidal at 10Hz, but insufficient at 100Hz.

From the methods that uses magnitude it is shown that the total impedance is decreasing with higher position in an almost linear way. This is changed when a base duty cycle is applied and even for a low base duty cycle the position signal at 0mm is changed drastically. This is because saturation hits the 0mm position first since there is no air gap and the magnetic flux can saturate the core at a low current.

In the theory section, it was stated that hysteresis was one of the core losses, but to investigate hysteresis between positions a different setup would be required. The case where hysteresis comes from switching polarities on the solenoid was not investigated due to it is not encountered unless someone manually changes it which is not supposed to happen.

6

Conclusion and future work

6.1 Conclusion

Methods

The best method was FC. Phase-based methods were the only methods with monotonic behavior while the solenoid was actuated. The monotonic behaviour is critical to be able to have a working position detection and therefore a phase-based method has to be used. The phase-based methods also had a very limited temperature dependency and were almost supply voltage independent. Although integration and FC magnitude had less variation per position it did not work well at the holding current. At high current (around 2A) even the phase-based methods could not distinguish the low positions properly. When high current (around 2A) is used a possible solution would be to use both magnitude-based and phase-based methods. In this case FC is definitely the best option, since it can provide both for almost no additional computation power. At a very high current (around 5.5A) phase cannot be used at all but then magnitude has distinguished positions. Current control was the only method throughout this thesis that could control the current and not only rely on a fixed duty cycle to get the desired current level.

Reflections

Reflecting back on the background and the goals, the position can be detected using different methods, most notably FC. The required position update of at most 100ms is also possible to achieve using any of the methods. The voltage range of 36-65V was only briefly investigated.

6.2 Future work

In the future diagnostics and ways to handle errors should be implemented. There should also be a closed-loop controller for the current. When using the FC method, the closed-loop controller could control the base duty cycle to keep the sinusoidal scan signal intact. The closed-loop current controller is needed because the solenoids can differ between units, and the holding-mode needs a certain current to keep the spring compressed. With another setup, hysteresis between positions could be investigated, this is relevant since hysteresis could affect the position measurement in a negative way. One way to do this is having a fix position and measure the difference in position signal at the position after a big current have been passed through the solenoid compared to when measuring after no current been flowing through. Another thing that should be taken into account in the future is the impact of disturbances, for example to investigate what kind of impact an induced sinusoidal with frequency close to the scan signal would have. The current PWM frequency of 2500Hz creates an audible noise and this could be solved with a higher PWM frequency (20kHz and higher). If the magnitude is to be used the duty cycles have to be scaled with the voltage. The model should also compensate for the temperature, one way to do this is to estimate the DC resistance. The DC resistance can be estimated by replacing the sinusoidal scan signal with a fixed voltage and then measure the current. With this resistance the temperature could be estimated using (2.7). To use this solenoid for its purpose the code could be implemented to have three state where state one is open, state two engage the plunger using a high current and state three is the holding-mode and uses the base duty cycle to keep the spring compressed.

References

Armstrong, K. (2018). *Skin effect and surface currents*. https://incompliancemag.com/article/skin-effect-and-surface-currents. Accessed on 2019-07-24.

Bekele, A. (2016). *Cooley-tukey fft algorithms*. http://people.scs.carleton.ca/~maheshwa/courses/5703COMP/16Fall/FFT_Report.pdf. Accessed on 2019-05-09.

Bruyne, P. D. and B. Currat (2015). *Temperature and frequency effects on cable resistance*. https://www.aesa-cortaillod.com/fileadmin/documents/knowledge/AN_150617_E_Snapshots_multimaterials.pdf. Accessed on 2019-05-22.

Cheng, D. K. (2013). *Field and Wave Electromagnetics*. 2nd Edition. Pearson Education, Edinburgh Gate, Harlow, Essex, CM20 2JE, GB.

Dee, J. (2013). *Pulse width modulation*. https://learn.sparkfun.com/tutorials/pulse-width-modulation/all. Accessed on 2019-07-29.

Eckenfels, T., F. Kolb, S. Lehmann, W. Neugebauer, and M. Calero (2018). *48 v hybridization a smart upgrade for the powertrain*. http://schaeffler-events.com/symposium/lecture/h3/index.html#oben. Accessed on 2019-07-29.

Elm, S. (2019). *Cascade matched filtering & adaptive threshold techniques on optical tracking signals under awgn*. http://lup.lub.lu.se/luur/download?func=downloadFile&recordOId=8974707&fileOId=8974708. Accessed on 2020-03-20.

Fitzpatrick, R. (2007a). *Energy stored in an inductor*. http://farside.ph.utexas.edu/teaching/3021/lectures/node103.html. Accessed on 2019-08-12.

Fitzpatrick, R. (2007b). *Self inductance*. http://farside.ph.utexas.edu/teaching/3021/lectures/node102.html. Accessed on 2019-08-12.

Fung, D. (2014). *Hybrids explained: mild v full v plug-in v extended range electric vehicle*. https://www.caradvice.com.au/279850/hybrids-explained-mild-v-full-v-plug-in-v-extended-range-electric-vehicle. Accessed on 2019-05-09.

Konda, S., Y. Yoshida, and O. Ichinokura (2017). *Eddy current loss evaluation of magnetic powder core based on electric and magnetic networks*. https://aip.scitation.org/doi/full/10.1063/1.4978587. Accessed on 2019-07-29.

Krantz, D. (-). *What is a flyback diode?* https://www.douglaskrantz.com/ElecFlybackDiode.html. Accessed on 2019-07-18.

Lynch, A. J. (2009). *Magnetic flux leakage robotic pipe inspection: internal and external methods*. http://citeseerx.ist.psu.edu/viewdoc/download?doi=10.1.1.594.2964&rep=rep1&type=pdf. Accessed on 2019-07-23.

McAllister, W. (2016). *Rl natural response*. https://www.khanacademy.org/science/electrical-engineering/ee-circuit-analysis-topic/ee-natural-and-forced-response/a/ee-rl-natural-response. Accessed on 2019-05-17.

Potlabathini, A. (2015). *Facility electrical losses: proximity effect, skin effect, and eddy current losses*. https://www.slideshare.net/abhinaypotlabathini/proximity-effect. Accessed on 2019-07-28.

Spazini, L. (2001). *Using copper pcb etch for low value resistance*. http://www.ti.com/lit/an/slua236/slua236.pdf. Accessed on 2019-07-23.

Spors, S. (2015). *Digital signal processing*. https://dsp-nbsphinx.readthedocs.io/en/nbsphinx-experiment/nonrecursive_filters/fast_convolution.html. Accessed on 2019-05-17.

Teja, R. (2018). *Schottky diode – working, characteristics, applications*. https://www.electronicshub.org/schottky-diode-working-characteristics-applications/#comments. Accessed on 2019-07-19.

Urbaniak, M. (2012). *Magnetic hysteresis andbasic magnetometry*. http://www.ifmpan.poznan.pl/~urbaniak/Wyklady2012/urbifmpan2012lect3_02.pdf. Accessed on 2019-10-16.

Weisstein, E. (2019a). *Covariance*. http://mathworld.wolfram.com/Covariance.html. Accessed on 2019-05-10.

Weisstein, E. (2019b). *Fast fourier transform*. http://mathworld.wolfram.com/FastFourierTransform.html. Accessed on 2019-05-08.

Whiteley, M. (2002). *Natural response of first order rc and rl circuits*. http://info.ee.surrey.ac.uk/Teaching/Courses/ee1.cct/circuit-theory/section6/natresponse.html. Accessed on 2019-07-29.

Wojes, R. (2019). *What is annealing in metallurgy?* https://www.thebalance.com/annealing-explained-2340013. Accessed on 2019-07-23.

A

Appendix

A.1 Driver

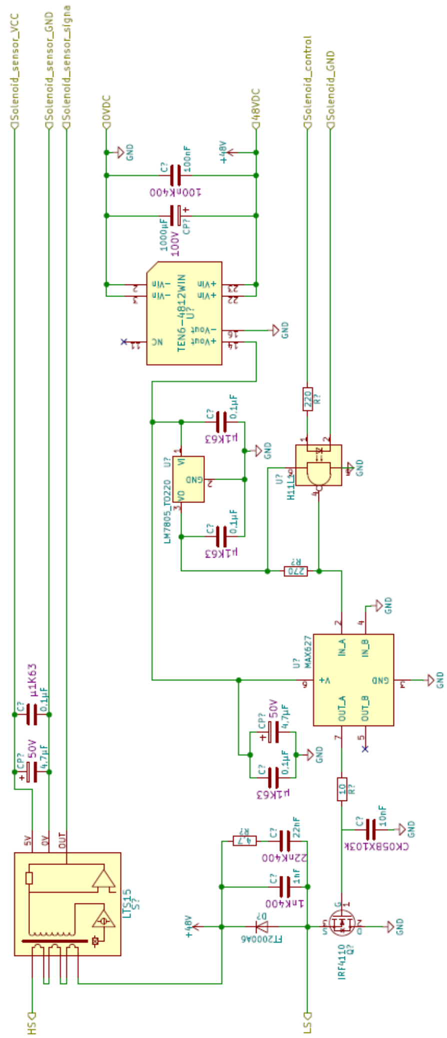

Figure A.1 The circuit diagram of the driver. This driver was used to amplify the 5V PWM signal from the MAB to the power supply voltage level. It also contain the flyback diode and the current sensor.

A.2 Simulink model

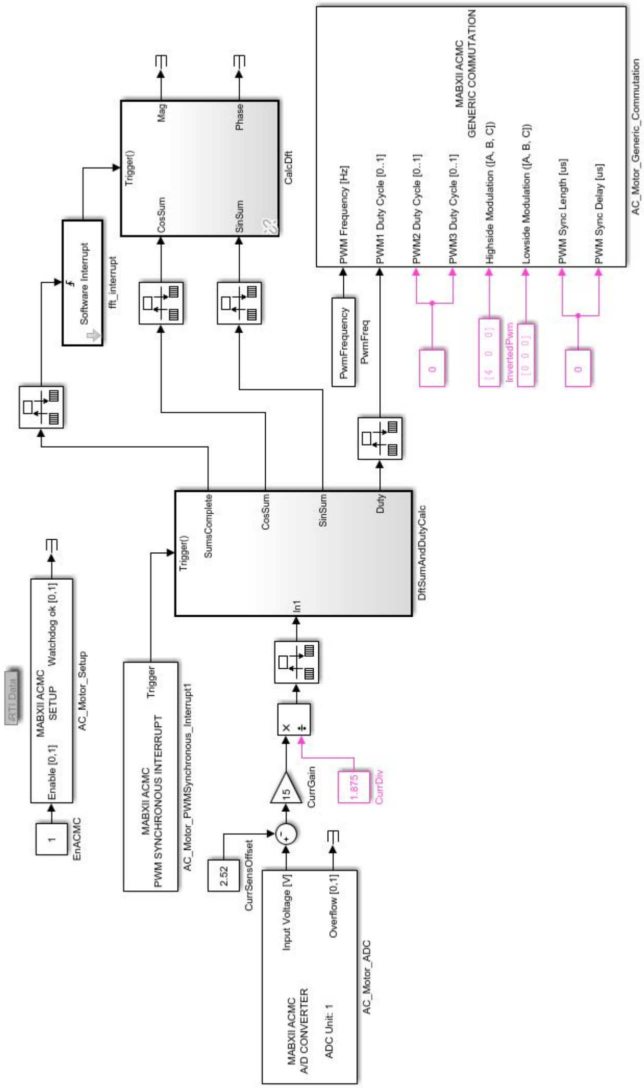

Figure A.2 The first layer of the simulink model FCmain. This is the layer that contains the ADC and PWM block.

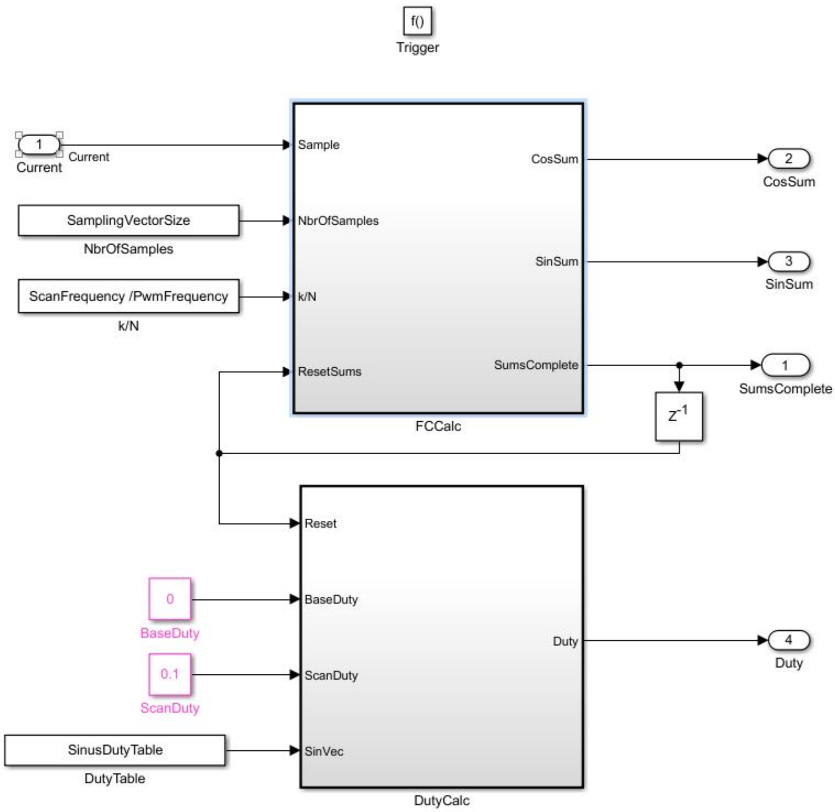

Figure A.3 This figure shows the subsystem FCAndDutyCalc and shows the relation between FCCalc and DutyCalc.

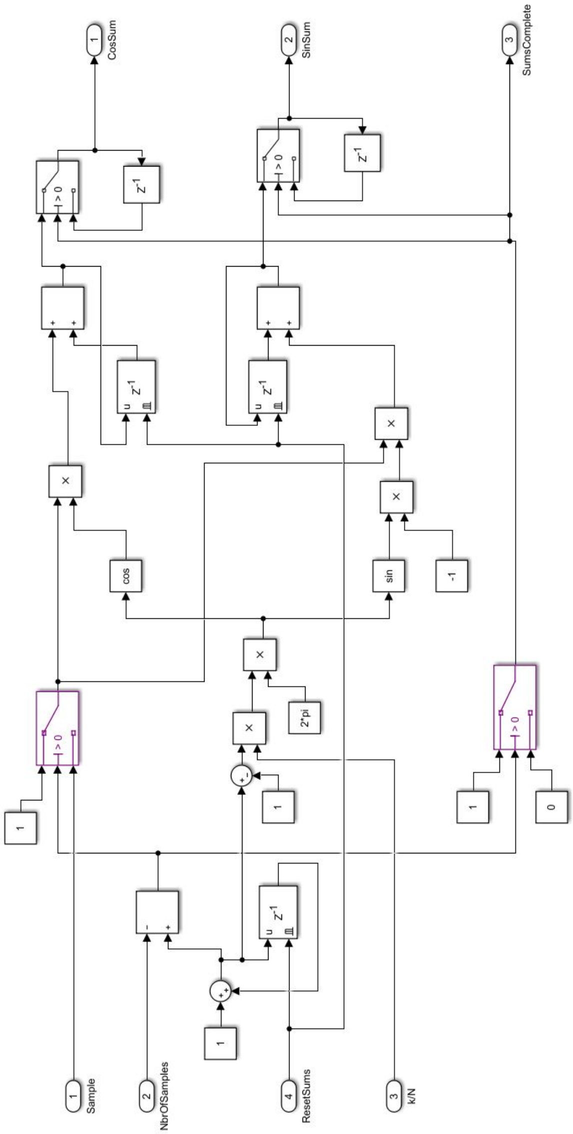

Figure A.4 This figure shows the subsystem FCCalc inside the subsystem FCAndDutyCalc where the FC are calculated.

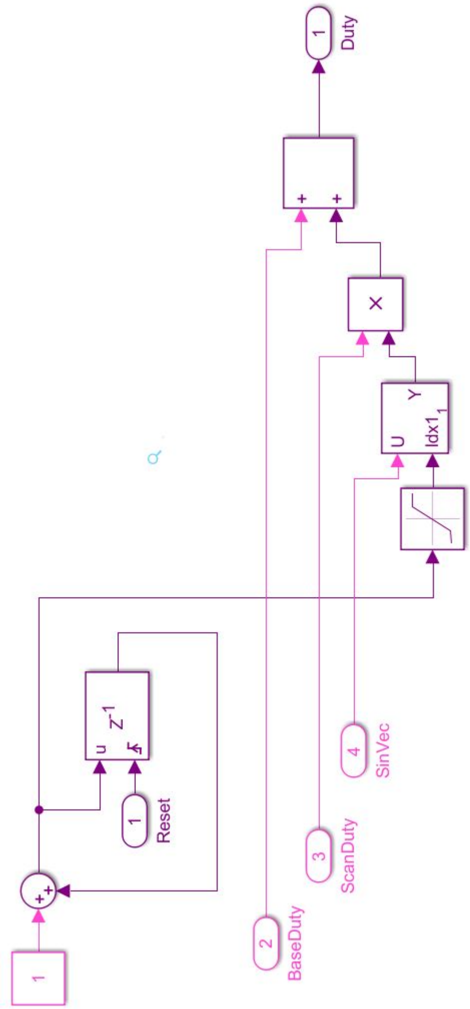

Figure A.5 This figure shows the subsystem DutyCalc inside the subsystem FCAn-dDutyCalc where the duty cycle is calculated using the base duty percentage added on to the sine duty multiplied with a value from the sine vector.

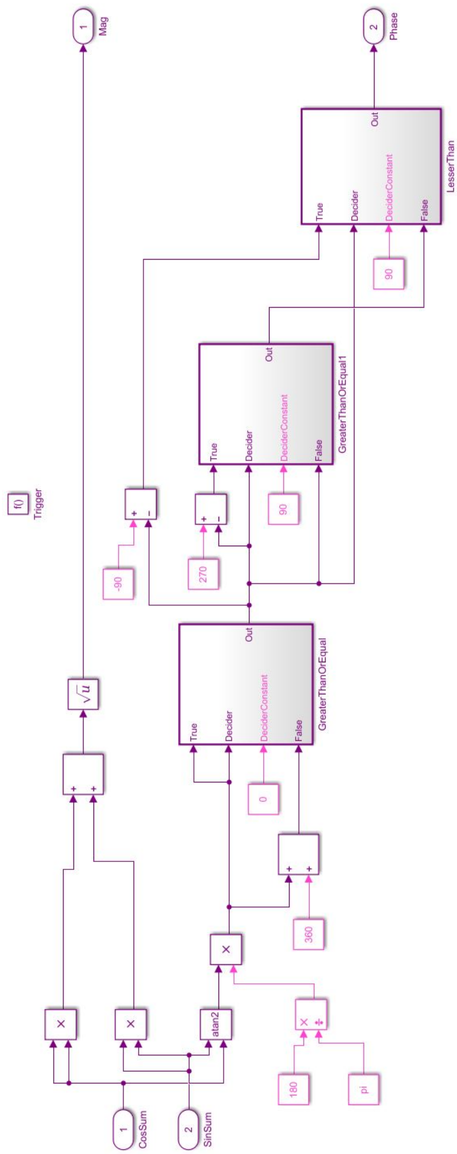

Figure A.6 This figure shows the subsystem ExtractPhaseMag where the phase and magnitude is calculated using the Trigonometric Function block with atan2 as function for phase and Sqrt block for magnitude. The blocks used after the Trigonometric Function is there to rescale the phase to the interval $0-360^{\circ}$.

Lund University
Department of Automatic Control
Box 118
SE-221 00 Lund Sweden

Document name
MASTER'S THESIS

Date of issue
April 2020

Document Number
TFRT-6097

Author(s)
Simon Hed
Axel Knutsson

Supervisor
Johan Blomberg, , BorgWarner
Arne Hörberg, BorgWarner
Anders Robertsson, Dept. of Automatic Control, Lund University, Sweden
Rolf Johansson, Dept. of Automatic Control, Lund University, Sweden (examiner)

Title and subtitle
Sensorless method of detecting plunger position in solenoid actuators

Abstract

This thesis investigates if it is possible to measure the plunger position in a Ledex 282352-023 solenoid actuator without the use of external sensors. To do this, various different methods, all based on comparing the current response to the applied voltage were evaluated from different categories such as calculation time, reliability and distinct position levels. The method that performed best in these categories was to calculate the phase difference between the voltage and the current using Fourier coefficients (FC). Model-based programming with MATLAB and Simulink was used to evaluate the performance of the methods. The Simulink model which implemented FC as measurement method is described in detail in this thesis. To run the models in real-time, hardware and software from dSpace were used which includes a MicroAutoBox II (MAB) and the program ControlDesk. This thesis was conducted in collaboration with BorgWarner.

Keywords

Classification system and/or index terms (if any)

Supplementary bibliographical information

ISSN and key title
0280-5316

ISBN

Language
English

Number of pages
1-92

Recipient's notes

Security classification

http://www.control.lth.se/publications/